A

PROJECT REPORT

ON

"SIZE CONTROLLED SYNTHESIS OF FERROMAGNETIC FERRUS PLATINUM (FePt) NANOPARTICLES BY CHEMICAL REDUCTION."

SUBMITTED BY

HARSH NARAYAN SINGH

(M.TECH NANOSCIENCE AND TECHNOLOGY)

(ROLL NO: 03/NST/09)

DELHI TECHNOLOGICAL UNIVERSITY
(FORMERLY DELHI COLLEGE OF ENGINEERING)

PREPARED AT

NATIONAL PHYSICAL LABORATORY (NPL)

Dr. K.S. KRISHNAN MARG, NEW DELHI

2011

ACKNOWLEDGEMENT

Now the final report is in my hands. It is not a one night venture; it requires determination, dedication, warmth bliss and grace of the Formless one that equips me to perform this task.

A formal statement of acknowledgement will hardly meet the end of justice while writing these words, I feel obliged to all of them who extended their inconceivable co-operation towards the achievement of whatever we have achieved.

First of all I would like to express deep sense of gratitude and sincere thanks to my supervisors **Dr. Renu Pasricha, Scientist E-II, and Dr Anurag Gupta Scientist E I**, **NPL, New Delhi** for providing experimental arrangements and making available literature and computer facility. A deep sense of gratitude is expressed to **Dr. Sukhvir Singh, Scientist E-II Head of Electron And Ion Microscopy Group, NPL, New Delhi** for his contribution to this work. Constant supervision of my guide throughout the project, learned guidance and invaluable suggestions helped me to complete the project well in stipulated time.

With due regards, I express sincere thanks to**Dr. R. K. Sinha, Head of Applied Physics Department, DELHI TECHNOLOGICAL UNIVERSITY, BAWANA ROAD,NEW DELHI,** for his valuable suggestions and support to attend NPL which enabled me to complete the project well in stipulated time.

I express my sincere thanks to **Dr. R.C. Budhani Director NPL,and Dr. Rajeev Chopra, HRD Group, NPL,** for allowing me to do my M.Tech research project at NPL.

I am deeply overwhelmed to my lab mate **Mohammad Umar, Sonal Singh, Stalin, Sanju Tanwar** for helping and kind attitude. Their appreciation and encouragement in all respect are really unforgettable for me**.**

Finally I would like to thank my parents and other family members who were always anxious to help me & contributed a major driving force behind the completion of this project.

HARSH NARAYAN SINGH

DECLARATION

I hereby declare that the present work entitled **"SIZE CONTROLLED SYNTHESIS OF FERROMAGNETIC FERRUS PLATINUM (FePt) NANOPARTICLE BY CHEMICAL REDUCTION."** has been completed by me under the privileged supervision of **Dr. Renu Pasricha, Scientist E-II of Electron And Ion Microscopy Group, NPL, New Delhi** for the fulfillment of the Degree of Master of Technology in Nanoscience And Technology. I have tried my level best, with earnest co-operation of some of my seniors and colleagues in a very informative manner. I hereby ensure that work done is authentic and is not a copy of previous work.

HARSH NARAYAN SINGH

CERTIFICATE

This is to certified that **Mr. Harsh Narayan Singh** final year student of **M.Tech Nanoscience And Technology** in the department of Applied physics of **Delhi Technological University** has successfully completed a thesis entitled **"SIZE CONTROLLED SYNTHESIS OF FERROMAGNETIC FERRUS PLATINUM (FePt) NANOPARTICLE BY CHEMICAL REDUCTION"** under the supervision of **Dr. Renu Pasricha** at Electron And Ion Microscopic Group,National Physical laboratory **(NPL)**, New Delhi.

This Thesis work has been carried out during July, 2010 to June, 2011.

Dr. Renu Pasricha
Scientist E-II

Dr Anurag Gupta
Scientist E I

Dr. Sukhvir Singh
Head, Scientist E-II

Electron And Ion Microscopic Group,
National Physical Laboratory,
Pusa Road, New Delhi.

TABLE OF CONTENTS

PROJECT OVERVIEW

Title: SIZE CONTROLLED SYNTHESIS OF FERROMAGNETIC FERRUS PLATINUM (FePt) NANOPARTICLES BY CHEMICAL REDUCTION.

OBJECTIVE:

1. SYNTHESIS OF FePt NANOPARTICLE BY SUPERHYDRIDE REDUCTION OF $FeCl_2$ AND $Pt(acac)_2$ AT HIGH TEMPERATURE.
2. SYNTHESIS OF FePt NANOPARTICLE BY AQUEOUS ROUTE.

ABSTRACT:

Ferromagnetic nanoparticles with uniform size distribution have drawn great attention in the past decades because of their unique magnetic properties and potential applications in high density recording media, exchange-spring permanent magnets and biotechnology. In this thesis, synthesis and characterization of ferromagnetic nanoparticles (FePt) are reported.

FePt nanoparticles with different sizes and compositions were successfully synthesized via chemical synthesis in the presence of different surfactants. In organic medium FePt particle size was tuned to a range of from 2 nm to 4 nm. Whereas in Aqueous medium range of FePt particle size as 2nm to 3nm.

As-synthesized FePt particles were annealed by making Film of FePt nanoparticle using PEI polymer as surface binding agent by Thermal Annealing treatment in inert environment with various temperatures and time. It was found that FePt nanoparticles can be transferred from disordered *A*1 phase to ordered *L*10 phase in several seconds at above 600 ºC.

AFM Studies revealed that after annealing there is some particle agglomeration were observed.

For the nanoparticles, it was difficult to increase or even maintain the magnetic properties after annealing because of high oxidation affinity of nanoparticles.

Following characterization techniques were used:

A) HRTEM.
B) XRD.
C) PPMS.
D) EPR.
E) VSM.
F) AFM.

ABOUT THE ORGANISATION

HISTORICAL BACKGROUND

The National Physical Laboratory is one of the earliest national laboratories set up under the Council of Scientific & Industrial Research. Late Shri Jawaharlal Nehru laid the foundation stone of NPL on 4th January 1947. Late Dr. K.S. Krishnan, FRS, was the first director of the laboratory. The main building of the laboratory was formally opened by Late Deputy Prime Minister, Sardar Vallabhbhai Patel on 21st January 1950.

OBJECTIVE

To strengthen and advance physics-based R&D for the overall development of Science and Technology in the country.

To establish, maintain and improve continuously by research, for the benefit of the nation, National Standards of Measurements and to realize the Units based on International System (Under the subordinate Legislations of Weights and Measures Act 1956, reissued in 1988 under

the 1976 Act). To identify and conduct after due consideration, research in areas of physics which are most appropriate to the needs of the nation and for advancement of field.

To assist industries, national and other agencies in their developmental tasks by precision measurements, calibration, development of devices, processes, and other allied problems related to physics.

AIMS AND OBJECTIVES

To identify and conduct, after due consideration, research in areas of Physics, which are most appropriate to the needs of the nation and for the advancement of the field.

To establish, maintain and improve continuously by research, for the benefit of the national, National Standards of Measurement, and to realize units based on International System.

To assist industries, national and other agencies in their developmental tasks by precision measurement, calibration, development of devices, processes and other allied problems related to Physics.

MAIN ACTIVITIES

- Research and development
- Sponsored and contact research
- Consultancy
- Calibration and testing

AREAS OF RESEARCH

- Measurement Standards
- Materials Science
- Materials Characterization
- Radio and Atmospheric Science
- Superconductivity and Cryogenics

SERVICE TO NATION

- Time keeping service to the nation
- Infrastructure for quality support in Metrology for commerce and trade
- National Metrology Institute for training and education
- New materials for engineering, electronic, commercial and medical applications
- New materials of strategic importance
- Key partner in establishing MST radar at Tirupati
- R&D backed service for making radio telecommunication disturbance free
- SODAR Technology
- Sustaining Indian presence in Antarctica by continuing atmospheric exploration
- Emerging as a center of pride and excellence for research and development work in Physics and related areas
- Preservation of the original manuscript of the constitution of the republic of India in a special chamber.

SERVICE TO INDUSTRY

- Sophisticated instrument facilities for characterization and testing of materials
- Testing and Calibration service
- Consultancy and Collaboration in a range of technology development areas
- Training and Education in Metrology
- Supplying Indian Critical Reference Materials
- Project Oriented Research
- Access to Information and Data Bases on R&D in Physics and related areas.

CHAPTER 1

FUNDAMENTAL OF MAGNETISM AND MAGNETIC MATERIALS

1.1 Basics of magnetism:

1.1.1 PHYSICAL ORIGIN OF MAGNETISM.

Magnetism describes phenomenon of forces between two or more objects that are related to a magnetic field.[1] This magnetic field is created by the movements and interactions of electrons. A magnet is an object that exhibits an external magnetic field and can be categorized into electromagnets and permanent magnets.[2] An electromagnet is a type of magnet in which the magnetic field is produced by the flow of an electric current in a wire. In contrast, a permanent magnet is a type of magnet in which the magnetic moments of the orbital electrons are aligned.[3,4] Therefore each atom can be considered as a tiny magnet. The electromagnetic field disappears when the current is removed, while a permanent magnet retains its magnetism for a long time without an external magnetic field. For the permanent magnets, the orbital electron creates the magnetic moment by moving around a nucleus (**Figure 1.1**).There is also a spin magnetic moment which is caused by a spin of electron itself. However, in most materials except a few elements (iron, cobalt, and nickel), there is no net magnetic moment because in pairs of electrons the magnetic moment is cancelled by its neighbor.

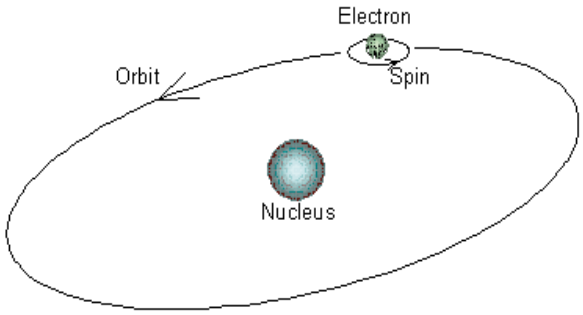

Figure 1.1 Orbit of a spinning electron about the nucleus of an atom

1.1.2 MAGNETIC FIELD AND MAGNETIC MOMENT.

The magnetic field strength is expressed by *H*. Here the magnetic flux density *B*, which is defined in terms of force on moving charge in the Lorentz force law, is shown as follow,

$$\boldsymbol{B = H + 4\pi M} \qquad \textbf{(1.1)}$$

where, *M* is called magnetization which is explained as the total magnetic moment *m* in unit volume. The units of magnetic properties are shown in **Appendix A**.

The magnetic properties of materials can be characterized not only by the magnitude of *M*, but also the magnitude of *M* change by varying *H*.[4] The ratio between *M* and *H* is called susceptibility χ,

$$\boldsymbol{\chi = M/H} \qquad \textbf{(1.2)}$$

Also the permeability is a similar quantity as the susceptibility and defined as,

$$\boldsymbol{\mu = B/H} \qquad \textbf{(1.3)}$$

The type of magnetism can be characterized by observing the susceptibility and permeability of a material.

1.2 Different types of magnetic behavior:

The types of magnetic behavior can be classified by knowing the materials response to applied magnetic field. **Figure 1.2** shows the summary of different types of magnetic behavior, including diamagnetism, paramagnetic and ferromagnetism in which anitferromagnetism and ferrimagnetisms are considered to be its subclasses.[4,6]

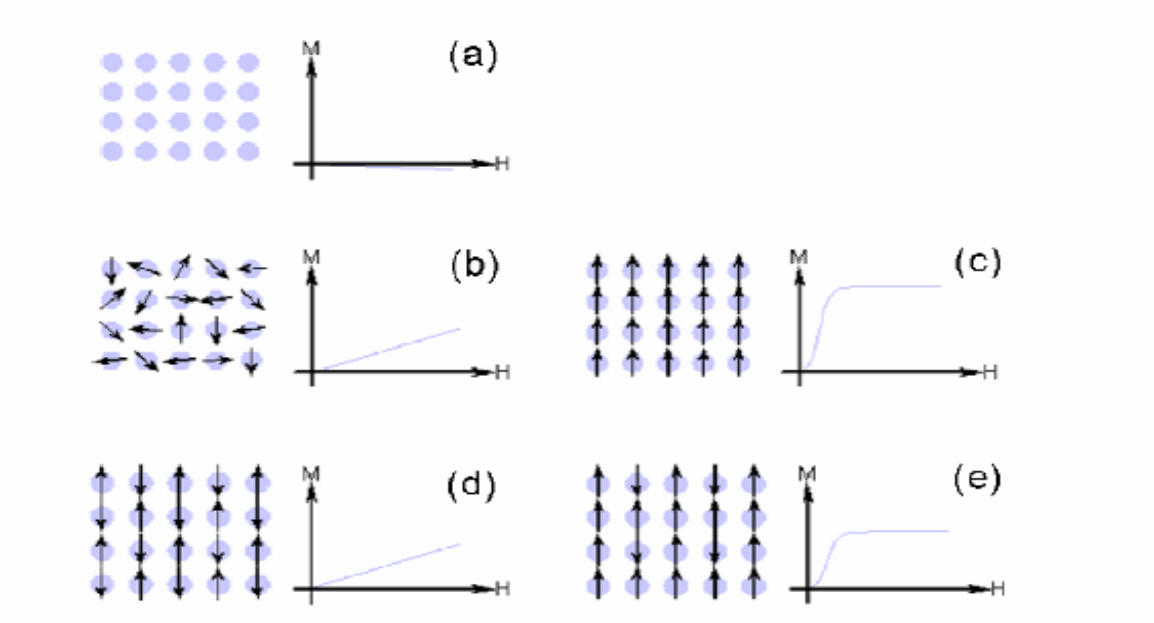

Figure 1.2 Summary of different types of magnetic behavior. Figure shows the direction of magnetic moment of each atom in the material and magnetization response to the magnetic field. **(a)** Diamagnetism, **(b)** paramagnetism, **(c)** ferromagnetism, **(d)** antiferromagnetism and **(e)** ferrimagnetisms.

1.2.1 DIAMAGNETISM.

Diamagnetic material shows no net magnetic moment if there is no external field. Under the applied field, the orbital electrons either accelerate or decelerate results in weak magnetic moment in the opposite direction to that of applied field. For diamagnetic materials, the susceptibility χ is small (order of 10^{-6}) and negative (Figure 1.2 (a)).

1.2.2 PARAMAGNETISM.

In paramagnetic materials, atoms have randomly oriented magnetic moments as shown in Figure 1.2 (b). Under the external magnetic field, some atoms in the material aligned their magnetic moment due to unpaired electrons in partially filled orbitals, resulting in the net magnetization and positive susceptibility (order of 10^{-5} to 10^{-2}). However, the net magnetic

moment goes to zero when the magnetic field is removed. As the temperature increases, the thermal agitation will increase and it will then become harder to align the atomic magnetic moments and hence the susceptibility will decrease.

1.2.3 FERROMAGNETISM.

Ferromagnetic materials exhibit a large net magnetization under the external magnetic field due to the parallel alignment of magnetic moments (Figure 1.2 (c)). The net magnetization originates from the overall contribution of magnetic moment in orbital electrons and its spins. In the periodic table of elements only Fe, Co and Ni are ferromagnetic at and above room temperature. The magnetic susceptibility can be reached up to 106 for ferromagnetic materials. However, when the ferromagnetic materials are heated up, the thermal fluctuation decreases the degree of alignment of magnetic moments, resulting in the decrease of magnetization. Eventually the thermal agitation becomes so great that the material becomes paramagnetic; the temperature of this transition is called the Curie temperature,$\mathbf{T_C}$.

1.2.4 ANTIFERROMAGNETISM.

In the periodic table the only element exhibiting antiferromagnetism at room temperature is chromium (Cr).Antiferromagnetic materials are very similar to ferromagnetic materials but the exchange interaction between neighbor atoms leads to the anti-parallel alignment of the atomic magnetic moments. Therefore, the magnetic field cancels out and the material appears to behave in the same way as a paramagnetic material (Figure 1.2 (d)). Like ferromagnetic materials these materials become paramagnetic above a transition temperature, known as the Néel temperature**,** $\mathbf{T_N}$.

1.2.5 FERRIMAGNETISM.

Ferrimagnetism is only observed in compounds, which have more complex crystal structures than pure elements. Within these materials the exchange interactions lead to parallel alignment of atoms in some of the crystal sites and anti-parallel alignment of others (Figure 1.2

(e)). The material breaks down into magnetic domains, just like a ferromagnetic material and the magnetic behavior is also very similar, although ferrimagnetic materials usually have lower saturation magnetizations. For example in Barium ferrite ($BaO.6Fe_2O_3$) the unit cell contains 64 ions of which the barium and oxygen ions have no magnetic moment, 16 Fe3+ ions have moments aligned parallel and 8 Fe3+ aligned anti-parallel giving a net magnetization parallel to the applied field, but with a relatively low magnitude as only 1/8 of the ions contribute to the magnetization of the material.

1.3 Ferromagnetic Properties:

1.3.1 MAGNETOCRYSTALLINE ANISOTROPY.

Most magnetic materials have the preference for the magnetization to lie in a particular crystalline direction, which is called magnetocrystalline anisotropy or crystalline anisotropy. In other word, magnetic anisotropy means the dependence of the magnetic properties on the direction in which they are measured. [7] For example, Fe has its easy axis in [100] direction, Ni (fcc) has its easy axis in [100] direction and Co (hcp) has its easy axis in [0001] direction (c-axis). Therefore the magnetic properties such as magnetization and coercivity are greatly affected by the magnetic anisotropy. The energy associated with the alignment of magnetization due to magnetic anisotropy is called anisotropy energy and given by,

$$E_a = K \sin^2\theta \qquad (1.4)$$

where θ is the angel between M_s and the easy axis and K is the anisotropy constant.

There are two important categories of magnetic anisotropy, magnetocrystalline anisotropy and shape anisotropy.

Magnetocrystalline anisotropy is intrinsic to materials while all other types of anisotropy are induced by processing methods. In magnetocrystalline anisotropy, the magnetization tends to orient itself along a preferred crystallographic direction called the easy axis. The

magnetocrystalline anisotropy energy can be defined as the energy difference between samples magnetized along easy and hard directions. One example of magnetocrystalline anisotropy like cobalt is shown in **Figure 1.3**.[8] The easy axis for Co is [0001] (i.e. along the c-axis), the final spontaneous magnetization is the same for both easy and hard directions but the applied field needed to reach that value is obviously different in each direction.

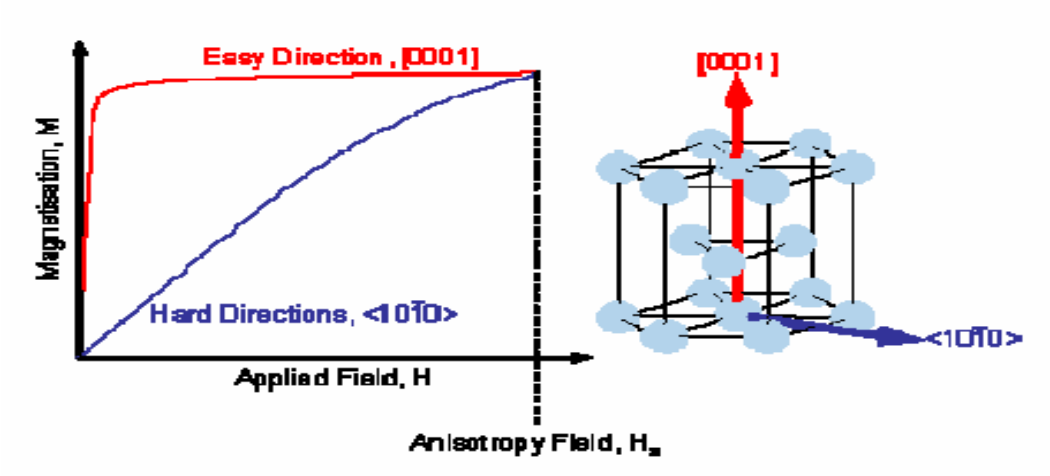

Figure 1.3 The magnetocrystalline anisotropy of cobalt

In contrast, although there is no preferred orientation in the polycrystalline sample, the magnetization will be easier to align along the long direction if the sample is not spherical. This phenomenon is called shape anisotropy. The shape anisotropy occurs due to the less demagnetization field along the long direction. For example, a long rod of iron with Ms = 1714 emu/cm^3 has a shape anisotropy constant Ks =1.85×10^7 erg/cm^3, which is much greater than many cases of magnetocrystalline anisotropy.[9]

1.3.2 HYSTERISIS LOOPS.

The hysteresis loops show the "history independent" nature of magnetization of ferromagnetic materials. As the applied field *H* increases, magnetization approaches to a saturation value *Ms*, which is called saturation magnetization **(Figure 1.4)**.The magnetization does not go back to zero when the field decreases to zero. Instead, it remains a certain value of magnetization when the field is zero, which is called remanence ***Mr***. When the magnetic field is applied in a reversed direction, magnetization reaches zero at a field magnitude called coercivity ***Hc***. Here the coercivity is the external energy needed to overcome the anisotropy energy. Further

increase of field in the reversed direction, the *M-H* curve follows the same behavior as the positive side.

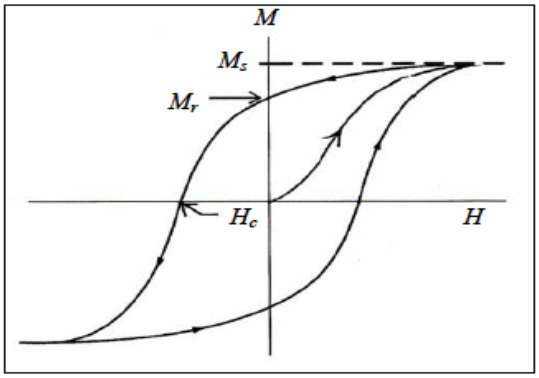

Figure 1.4 The typical illustration of full hysteresis loop. Ms is the saturation magnetization, *Mr* is the remanence magnetization and *Hc* is the coercivity

1.3.3 MAGNETIC DOMAIN.

Domain walls are boundaries between regions in which the magnetization has different directions. Within this wall, every magnetization must have different direction from one domain to the next domain. Domain walls have a finite width that is determined principally by exchange and magnetocrystalline anisotropy energy.

Exchange energy tends to keep magnetic moment parallel to each other and can be kept small if the 180 ° rotation takes place gradually with wide wall as shown in **Figure 1.5 (a),** but large with thin wall as shown in **Figure 1.5 (b).** However, for the wide wall structure, the magnetizations within the wall are no longer aligned along an easy axis of magnetization. This produces an anisotropy energy, which is high in (a) but low in (b). The exchange energy tends to make the wall as wide as possible whereas the anisotropy tends to make the wall as thin as possible. As a result of this competition between exchange and anisotropy energies, the domain wall has a finite width (on the order of 10 nm).

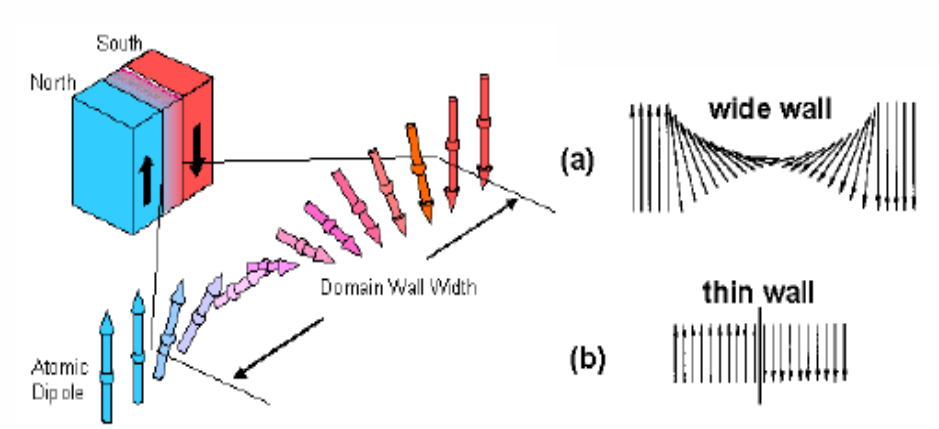

Figure 1.5 Schematic representation of a 180 º domain wall with **(a)** wide wall with gradual magnetization change, and **(b)** thin wall with abrupt magnetization change[8]

1.3.4 EXCHANGE COUPLED NANOCOMPOSITE MAGNETS.

In the *B-H* loop shown in **Figure 1.6**, the maximum product value of *B* and *H* is called the maximum energy product *(BH)max*, which is a parameter to demonstrate the maximum work that can be done by the permanent magnet. Large coercivity *Hc* and saturation magnetization *Ms* result in large *(BH)max*. For materials with sufficiently high *Hc* values (*Hc* > $2\pi Ms$), the theoretical limit of the energy product is,[10]

$$(BH)_{max} \leq (2\pi Ms)^2 \qquad (1.5)$$

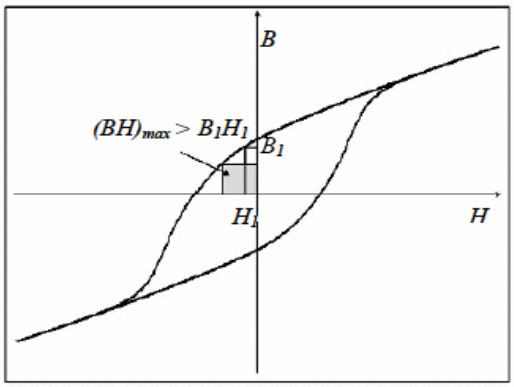

Figure 1.6 The typical B-H loop of ferromagnetic materials

As the hard magnetic materials are being developed, $(BH)_{max}$ has experienced a huge increase in the past one hundred years, as shown in **Figure 1.7**[11]. Driven by the theoretical limit of maximal energy product described by equation (1.5), huge efforts have been put into developing new hard magnetic materials with high anisotropy and magnetization. In 1991, Kneller and Hawig[12] proposed an alternative approach to enhance the energy product by making a nanocomposite of exchange-coupled hard and soft magnetic phases. The hard phase provides the high magnetic anisotropy and stabilizes the exchange-coupled soft phase against demagnetization and the soft phase provides the high magnetization to enlarge the maximal energy product $(BH)_{max}$, as shown in **Figure 1.8**.

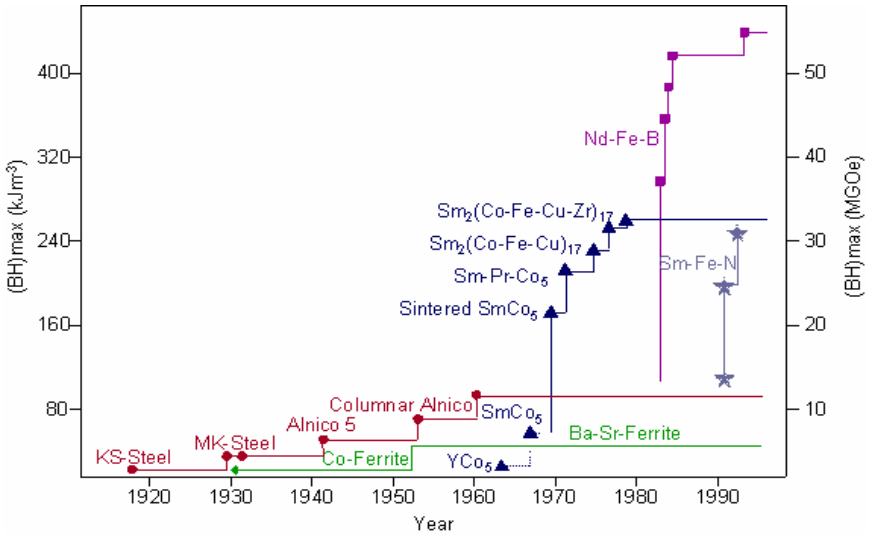

Figure 1.7 Evolution of $(BH)_{max}$ of permanent magnets in the 20th century

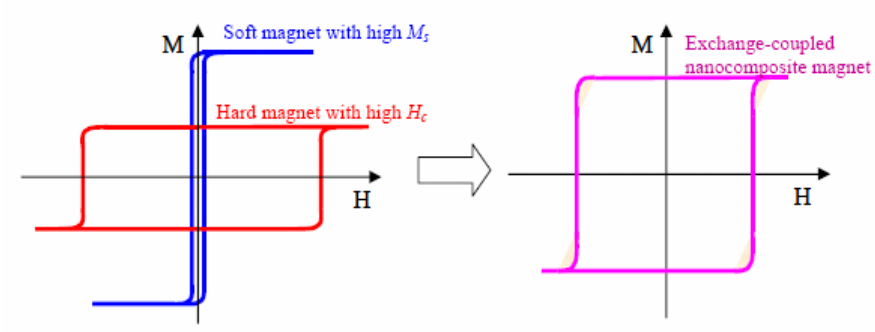

Figure 1.8 Hysteresis loops of soft, hard, and nanocomposite magnetic materials

In addition, micromagnetic simulations have predicted the possibility of huge increase in the maximum energy product $(BH)_{max}$ by using exchange-coupled nanocomposites. For FePt/Fe_3Pt exchange-coupled nanocomposites, the maximum energy products $(BH)_{max}$ about 34.6 MGOe can be obtained for the 3 nm scale isotropic magnets with the volume fraction of soft Fe_3Pt phase vs = 15 % [13]. Moreover, it was reported that anisotropic nanocomposite permanent magnets composed of hard and soft magnetic phases can potentially be reached the $(BH)_{max}$ of 100 MGOe [14]. For example, in $Pr_2Fe_{14}B$/a-Fe and $Sm_2Fe_{17}N_3/Fe_{65}Co_{35}$ nanocomposites, the maximum $(BH)_{max}$ of 33 and 40 MGOe can be obtained in the isotropic permanent magnets, while 101 and 112 MGOe[15] can be obtained for the anisotropic permanent magnets, respectively, implying that the alignment of the easy axis of hard phase is necessary for high performance.

1.4 Ferromagnetic Materials:

1.4.1 SOFT MAGNETIC MATERIALS.

There are two categories for ferromagnetic materials, soft magnetic and hard magnetic materials, according to their hysteresis properties **(Figure 1.9)**. Soft magnetic materials need low strength of external magnetic field to be magnetized and demagnetized. Therefore, relatively, soft magnetic materials have low coercivity, typically less than 10 Oe, high saturation magnetization *Ms* but low remanence *Mr*, as shown in Figure 1.5.

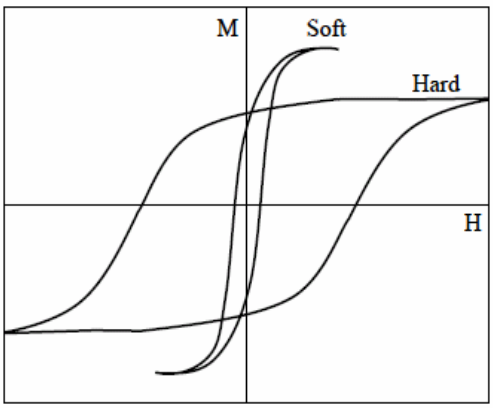

Figure 1.9 Hysteresis loops of typical hard and soft magnetic materials

1.4.2 HARD MAGNETIC MATERIALS.

The term "hard" means that hard magnetic materials are more difficult to be demagnetized than soft magnetic materials. Therefore, it requires higher magnetic field to be demagnetized to zero, which indicates that the coercivity is higher. In fact, the relatively high coercivity, which is usually larger than 1000 Oe, is the criteria of hard magnetic materials, as shown in Figure 1.5.Also, the remaining magnetization is relatively large after removal of the magnetizing field, which means that the hard magnetic materials have higher remanence *Mr*. Because of this ability to store magnetization in the absence of magnetic field, hard magnetic materials are also known as permanent magnetic materials. The most well known hard magnetic materials are cobalt-rare earth alloys ($SmCo_5$ and Sm_2Co_{17}), neodymium-iron-boron ($Nd_2Fe_{14}B$), iron-platinum (FePt), cobalt-platinum (CoPt), hard ferrites ($SrO\text{-}Fe_2O_3$ or $BaO\text{-}6Fe_2O_3$) and Alnicos.

1.5 Magnetic nanoparticles:

1.5.1 SINGLE DOMAIN PARTICLES.

The magnetostatic energy of a material could be decreased by restructuring it into domains [4,7].Because it needs energy to complete the formation of domains, in large volume of particles there would be a minimum domain size below which the energy needed for domain formation exceeds the benefits from decreasing the magnetostatic energy. This means a single particle with size comparable to the minimum domain size will not break into domains and remains single domain [4,7].

The magnetization of a single-domain particle lies along the easy axis direction in the absence of applied magnetic field. When a field is applied opposite to the direction of the magnetization, the magnetic moments rotate through the hard direction to a new easy direction. There is no domain structure change with this magnetization switching. It is always more difficult to overcome the anisotropy force that holds the magnetization in the easy direction to rotate the magnetization

than to move a domain wall, thus, single-domain particles have a larger coercivity than multi-domain materials, as shown in **Figure 1.10**.

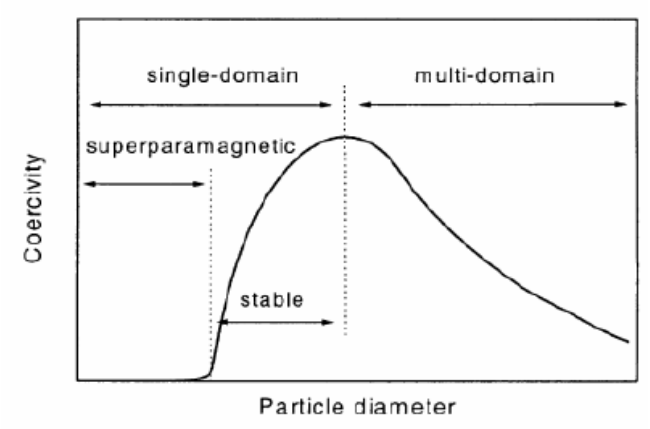

Figure 1.10 Coercivity dependence on particles diameter

1.5.2 SUPER-PARAMAGNETISM.

Super-paramagnetism occurs when the material is composed of very small single-domain particles (1-10 nm). The anisotropy energy is the energy required to change the direction of magnetization of a particle and is given by,

$$Ea=KV \qquad (1.6)$$

where K is the anisotropy energy density and V is the volume of the particle. When the particle size decreases below a critical size, the thermal energy is sufficient to overcome the anisotropy energy of the particle even the temperature is below the Curie temperature. This results in thermal fluctuation in the direction of magnetization as shown in **Figure 1.11** and the particle behaves like the paramagnetism, except that the magnetic moments of the entire crystallite tend to align under the magnetic field instead of each individual atom being independently influenced by an external magnetic field.

Figure 1.11 Illustration of super-paramagnetic effect

1.6 Applications of Magnetic Nanoparticles:

Depending on type of applications, magnetic nanoparticles are used in varieties of forms such as surface functionalized particles in biomedical applications, as particles arrays in magnetic storage media, as compacted powders in permanent magnets and in solutions as ferrofluids.

1.6.1 BIOMEDICAL APPLICATION.

Magnetic nanoparticles have been proposed for biomedical applications for several years. In recent years, nanotechnology has developed to a stage that makes it possible to produce, characterize and specifically tailor the functional properties of nanoparticles for applications.This shows considerable promise for applications in biomedical and diagnostic fields such as targeted drug delivery, hyperthermic treatment for malignant cell, and magnetic resonance imaging (**MRI**).There are three reasons why the magnetic nanoparticles are useful in biomedical applications. First, magnetic nanoparticles can have controllable size ranging from a few nanometers up to tens of nanometers, and are smaller than comparable in sizes to a cell (10-100μm), a virus (20-450 nm), a protein (5 -50 nm) or a gene (2nm wide and 10 -100 nm long). They can get close to the cell or gene and they can be coated with biomoleclues to make them interact or bind with biological entity. Second, magnetic nanoparticles can be manipulated by an external magnetic field gradient. They can be used to deliver a package, such as an anticancer drug to a targeted region of the body such as a tumor. Third, magnetic nanoparticles can also be made to resonantly respond to a time-varying magnetic field, with an associated transfer of energy from the field to the nanoparticles. They can be made to heat up, which leads to their use as hyperthermia agents, delivering toxic amounts of thermal energy to targeted bodies such as tumors or as chemotherapy.As highlighted above for biomedical application, magnetic nanoparticles must (i) have a good thermal stability; (ii) have a larger magnetic moment; (iii) be biocompatible; (iv) be able to form stable dispersion so the particles could be transported in living system; (v) response well to AC magnetic fields. Furthermore, better control of particle size and properties will be necessary to use these particles in biomedical application, in which uniformity of the properties will ensure accurate dosing and delivery. The widely used magnetic

nanoparticles for biomedical applications are magnetite (Fe_3O_4) and related oxides which are chemically stable, nontoxic, non-carcinogenic and have attractive magnetic properties.

1.6.2 MAGNETIC RECORDING MEDIA.

Synthesis and assembly of magnetic nanoparticles have attracted great attention because of their potential application in ultrahigh-density magnetic recording.Continue increase in the areal density of hard disk drive will be limited by thin film media in which each bit of information is stored over hundreds of grains. Self-assembled nanoparticle media and patterned media, in which data are stored in an array of single-domain magnetic particle have been suggested as means to overcome this limitation and to enable recording density up to 1 Tbit $inch^{-2}$.In such ultrahigh-density media, because of high recording density, a small material grain and narrow size distribution are required. To obtain both high signal-to-noise and thermal stability of the media, isolated, noninteracting or very weekly interacting nanoparticles with very high magnetic anisotropy energy K_u are required. Extensive researches are being done on $CoFe_2O_4$ and FePt nanoparticles for high density recording media. $CoFe_2O_4$ nanoparticles are well-known material with very high cubic magnetocrystalline anisotropy, good coercivity, and moderate saturation magnetization. These nanoparticles are one of the best candidates for ultrahigh density recording media with very high magnetocrystalline anisotropy (*K*is 10erg/cm), which is much higher than those of the currently used CoCr-based alloys. This large crystalline anisotropy allows for thermally stable grain diameters down to 2.8 nm. However, the as-synthesized FePt nanoparticles are superparamagnetic and have the face-centered cubic (fcc) structure. These particles have to be annealed at temperature as high as 580C to transform into face-centered tetragonal (fct) structure and retain magnetic orientation to be useful for recording. The post-annealing leads to poor control over arrangement of nanoparticles through extensive particle aggregation which also makes magnetic easy axes alignment difficult, limiting their technological applications. Recently, Liu et al. have made a break though by successfully preparing monodisperse FePt fct nanoparticles with high coercivity, which make it possible the direct application of fully converted fct FePt nanoparticles in high density magnetic media.

1.6.3 EXCHANGE COUPLED NANOCOMPOSITE MAGNETS.

Exchange-coupled nanocomposite magnet consists of a uniform mixture of exchange coupled magnetically hard and soft phases. This type of magnets are promising for advanced permanent magnetic applications as high energy products $(BH)_{max}$ and relatively high coercivities can be developed in these nanocomposite magnets. A small grain size (less than 20 nm) and a uniform mixture of the hard and soft phases are required for effective exchange coupling between the hard and the soft phases. Zeng *et al.* in 2002 demonstrated that exchange-coupled nanocomposite magnet such as FePt-Fe_3Pt can be made using monodisperse nanoparticles of FePt and Fe_3O_4 as precursors by self assembly technique. In exchange-coupled isotropic FePt-Fe_3Pt nanocomposite the energy product of 20.1 MGOe was achieved, which is 50% higher than that expected theoretically from a single phase, non-exchange-coupled isotropic FePt.

Recently, the same group prepared an exchange-coupled bimagnetic core/shell nanoparticles system with ferromagnetic FePt core and ferrimagnetic MFe_2O_4 (M=Fe, Co) shell. The advantage of this system is that the magnetic properties such as magnetization and coercivity can be controlled by tuning the core/shell dimensions, and by tuning the material parameters of both core and shell. This system shows the great promise for achieving the potential high energy products in exchange-coupled nanocomposite magnets. An anisotropic nanocomposite magnet with both the hard and soft phases aligned is expected to show much higher energy product than the isotropic one. However, controlling morphology including grain size and grain alignment in nanocomposite magnet remains a great challenge.

1.6.4 FERROFLUIDS.

A ferrofluid is a special solution of magnetic nanoparticles in a colloidal suspension whose flow can be controlled by magnets or magnetic fields. Particles are coated with a surfactant that disperse the particles and prevents agglomeration by overcoming the van der Waals forces that exists between the particles. As a result when fluid is not in presence of external magnetic field it has zero net magnetization. When a strong magnet is brought close to the ferrofluid, several spikes will appear, as the fluid arranges itself along the magnetic field

lines of the magnet. When the field is removed, the particles again disperse randomizing their orientation and establishing no net magnetization. These unique properties make ferrofluids have applications in numerous fields of technology. The most common application of ferrofluids is the cooling of loudspeakers. The ohmic heat produced in the voice coil can be transmitted to the outer structure by the fluid which increases the cooling approximately by a factor 3. In sealing technology, a drop of ferrofluid is put into the gap between a magnet and a high permeable rotating shaft. In the small gap a strong magnetic field fixes the ferrofluid, and pressure differences about 1 bar can be sealed without serious difficulties. Some of the other technological applications of ferrofluid include bearing, dampers, stepping motors, and sensors.

CHAPTER 2

CHARACTERIZATION TECHNIQUES

2.1 X-ray Diffraction (XRD):

X-ray scattering technique is a family of non-destructive analytical techniques which reveal information about the crystallographic structure, chemical composition, and physical properties of materials and thin films. These techniques are based on observing the scattered intensity of an X-ray beam hitting a sample as a function of incident and scattered angle, polarization, and wavelength or energy.

2.1.1 PRINCIPLES OF X-RAY POWDER DIFFRACTION (XRD)

Max von Laue, in 1912, discovered that crystalline substances act as three-dimensional diffraction gratings for X-ray wavelengths similar to the spacing of planes in a crystal lattice. X-ray diffraction is now a common technique for the study of crystal structures and atomic spacing.

X-ray diffraction is based on constructive interference of monochromatic X-rays and a crystalline sample. These X-rays are generated by a cathode ray tube, filtered to produce monochromatic radiation, collimated to concentrate, and directed toward the sample. The interaction of the incident rays with the sample produces constructive interference (and a diffracted ray) when conditions satisfy Bragg's Law ($n\lambda=2d \sin \theta$). This law relates the wavelength of electromagnetic radiation to the diffraction angle and the lattice spacing in a crystalline sample. These diffracted X-rays are then detected, processed and counted. By scanning the sample through a range of 2θangles, all possible diffraction directions of the lattice should be attained due to the random orientation of the powdered material. Conversion of the diffraction peaks to d-spacings allows identification of the mineral because each mineral has a set of unique d-spacings. Typically, this is achieved by comparison of d-spacings with standard reference patterns.

All diffraction methods are based on generation of X-rays in an X-ray tube. These X-rays are directed at the sample, and the diffracted rays are collected. A key component of all

diffraction is the angle between the incident and diffracted rays. Powder and single crystal diffraction vary in instrumentation beyond this.

Figure 2.1 XRD facility in NPL.

2.1.2 X-RAY GENERATION & PROPERTIES.

X-rays are electromagnetic radiation with typical photon energies in the range of 100 eV - 100 keV. For diffraction applications, only short wavelength x-rays (hard x-rays) in the range of a few angstroms to 0.1 angstrom (1 keV - 120 keV) are used. Because the wavelength of x-rays is comparable to the size of atoms, they are ideally suited for probing the structural arrangement of atoms and molecules in a wide range of materials. The energetic x-rays can penetrate deep into the materials and provide information about the bulk structure.

X-rays are produced generally by either x-ray tubes or synchrotron radiation. In a x-ray tube, which is the primary x-ray source used in laboratory x-ray instruments, x-rays are generated when a focused electron beam accelerated across a high voltage field bombards a stationary or rotating solid target. As electrons collide with atoms in the target and slow down, a continuous spectrum of x-rays are emitted, which are termed Bremsstrahlung radiation. The high energy electrons also eject inner shell electrons in atoms through the ionization process. When a free electron fills the shell, an x-ray photon with energy characteristic of the target material is

emitted. Common targets used in x-ray tubes include Cu and Mo, which emits 8keV and 14keV x-rays with corresponding wavelengths of 1.54 Å and 0.8 Å, respectively. (The energy E of an x-ray photon and its wavelength is related by the equation $E = hc/\lambda$, where h is Planck's constant and c the speed of light).

In recent years synchrotron facilities have become widely used as preferred sources for x-ray diffraction measurements. Synchrotron radiation is emitted by electrons or positrons travelling at near light speed in a circular storage ring. These powerful sources, which are thousands to millions of times more intense than laboratory x-ray tubes, have become indispensable tools for a wide range of structural investigations and brought advances in numerous fields of science and technology.

2.1.3 LATTICE PLANES AND BRAGG'S LAW.

X-rays primarily interact with electrons in atoms. When x-ray photons collide with electrons, some photons from the incident beam will be deflected away from the direction where they originally travel, much like billiard balls bouncing off one another. If the wavelength of these scattered x-rays did not change (meaning that x-ray photons did not lose any energy), the process is called elastic scattering (Thompson Scattering) in that only momentum has been transferred in the scattering process. These are the x-rays that we measure in diffraction experiments, as the scattered x-rays carry information about the electron distribution in materials. On the other hand, in the inelastic scattering process (Compton Scattering), x-rays transfer some of their energy to the electrons and the scattered x-rays will have different wavelength than the incident x-rays.

Diffracted waves from different atoms can interfere with each other and the resultant intensity distribution is strongly modulated by this interaction. If the atoms are arranged in a periodic fashion, as in crystals, the diffracted waves will consist of sharp interference maxima (peaks) with the same symmetry as in the distribution of atoms. Measuring the diffraction pattern therefore allows us to deduce the distribution of atoms in a material.

The peaks in x-ray diffraction pattern are directly related to the atomic distances. Let us consider an incident x-ray beam interacting with the atoms arranged in a periodic manner as

shown in 2 dimensions in the following illustrations.The face of a crystal lattice consists of parallel rows of atoms separated by a unique distance (d-spacing), which are capable of diffracting X-rays [16].

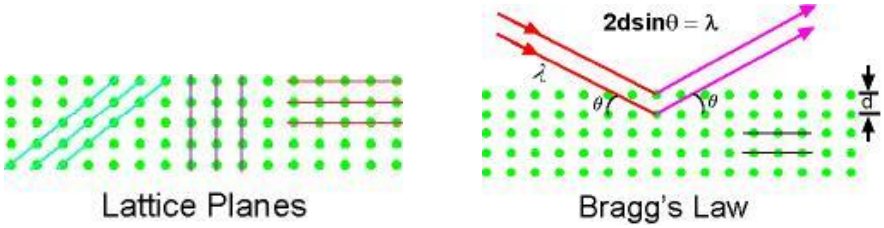

Figure 2.2 Lattice Planes and X-ray diffraction; θ is angle between incident radiation and scattering plane

The atoms, represented as spheres in the **Figure 2.2**, can be viewed as forming different sets of planes in the crystal (lines in graph on left). For a given set of lattice planes with an inter-plane distance of d, the condition for a diffraction (peak) to occur can be simply written as:

$$2d\sin\theta = n\lambda \qquad (2.1)$$

which is known as the Bragg's law, after W.L. Bragg, who first proposed it. In the equation, λ is the wavelength of the x-ray, θ the scattering angle, and n an integer representing the order of the diffraction peak. The Bragg's Law is one of most important laws used for interpreting x-ray diffraction data.

It is important to point out that although we have used atoms as scattering points in this example, Bragg's Law applies to scattering centers consisting of any periodic distribution of electron density. In other words, the law holds true if the atoms are replaced by molecules or collections of molecules, such as colloids, polymers, proteins and virus particles

2.1.4 POWDER DIFFRACTION.

Powder XRD (X-ray Diffraction) is perhaps the most widely used x-ray diffraction technique for characterizing materials. As the name suggests, the sample is usually in a powdery form, consisting of fine grains of single crystalline material to be studied. The technique is used

also widely for studying particles in liquid suspensions or polycrystalline solids (bulk or thin film materials).

The term 'powder' really means that the crystalline domains are randomly oriented in the sample. Therefore when the 2-D diffraction pattern is recorded, it shows concentric rings of scattering peaks corresponding to the various d spacings in the crystal lattice. The positions and the intensities of the peaks are used for identifying the underlying structure (or phase) of the material. For example, the diffraction lines of graphite would be different from diamond even though they both are made of carbon atoms. This phase identification is important because the material properties are highly dependent on structure (just think of graphite and diamond).

Powder diffraction data can be collected using either transmission or reflection geometry, as shown below. Because the particles in the powder sample are randomly oriented, these two methods will yield the same data.

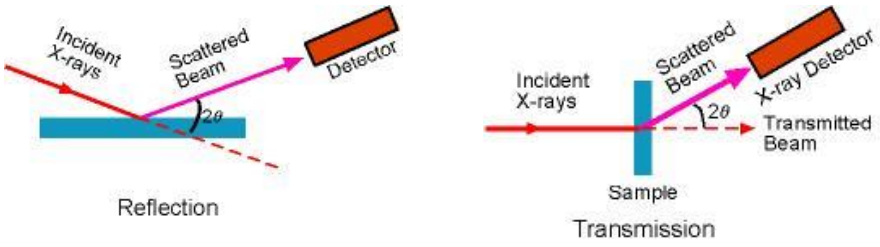

2.1.5 THIN FILM DIFFRACTION.Generally speaking thin film diffraction refers not to a specific technique but rather a collection of XRD techniques used to characterize thin film samples grown on substrates. These materials have important technological applications in microelectronic and optoelectronic devices, where high quality epitaxial films are critical for device performance. Thin film diffraction methods are used as important process development and control tools, as hard x-rays can penetrate through the epitaxial layers and measure the properties of both the film and the substrate.

There are several special considerations for using XRD to characterize thin film samples. First, reflection geometry is used for these measurements as the substrates are generally too thick for transmission. Second, high angular resolution is required because the peaks from semiconductor materials are sharp due to very low defect densities in the material. Consequently, multiple bounce crystal monochromators are used to provide a highly collimated x-ray beam for these measurements. Basic XRD measurements made on thin film samples include:

- Precise lattice constants measurements derived from 2θ - θ scans, which provide information about lattice mismatch between the film and the substrate and therefore is indicative of strain & stress
- Rocking curve measurements made by doing a θ scan at a fixed 2θ angle, the width of which is inversely proportionally to the dislocation density in the film and is therefore used as a gauge of the quality of the film.
- Superlattice measurements in multilayered heteroepitaxial structures, which manifest as satellite peaks surrounding the main diffraction peak from the film. Film thickness and quality can be deduced from the data.
- Glancing incidence x-ray reflectivity measurements, which can determine the thickness, roughness, and density of the film. This technique does not require crystalline film and works even with amorphous materials.

2.1.6 APPLICATION.

X-ray powder diffraction is most widely used for the identification of unknown crystalline materials (e.g. minerals, inorganic compounds). Determination of unknown solids is critical to studies in geology, environmental science, material science, engineering and biology. Other applications include:

- characterization of crystalline materials
- identification of fine-grained minerals such as clays and mixed layer clays that are difficult to determine optically
- determination of unit cell dimensions

- measurement of sample purity

With specialized techniques, XRD can be used to:

- determine crystal structures using Rietveld refinement
- determine of modal (average) amounts of minerals (quantitative analysis)
- characterize thin films samples by:
    - determining lattice mismatch between film and substrate and to inferring stress and strain
    - determining dislocation density and quality of the film by rocking curve measurements
    - measuring superlattices in multilayered epitaxial structures
    - determining the thickness, roughness and density of the film using glancing incidence X-ray reflectivity measurements
- make textural measurements, such as the orientation of grains, in a polycrystalline sample

2.1.7 STRENGTH AND LIMITATION OF X-RAY POWDER DIFFRACTION(XRD).

Strengths

- Powerful and rapid (< 20 min) technique for identification of an unknown mineral
- In most cases, it provides an unambiguous mineral determination
- Minimal sample preparation is required
- XRD units are widely available
- Data interpretation is relatively straight forward

Limitations

- Homogeneous and single phase material is best for identification of an unknown
- Must have access to a standard reference file of inorganic compounds (d-spacings, hkl s)
- Requires tenths of a gram of material which must be ground into a powder
- For mixed materials, detection limit is ~ 2% of sample

- For unit cell determinations, indexing of patterns for non-isometric crystal systems is complicated
- Peak overlay may occur and worsens for high angle 'reflections'

2.2 Electron Microscopy:

An electron microscope is a type of microscope that uses electrons to illuminate and create an image of a specimen. It has much higher magnification and resolving power than a light microscope, allowing it to see smaller objects and greater detail in these objects. In Light microscopes, the maximum resolution that one can image is determined by the wavelength of the photons that are being used to probe the sample. Visible light has wavelengths of 400–700 nanometres; larger than many objects of interest. Ultraviolet could be used, but there is a problem of absorption. Even shorter wavelengths, such as X-rays, exhibit a lack of interaction with the sample. On the other hand, the wavelength of electrons, which is dependent on their energy, can be tuned by adjustment of accelerating fields, and can be much smaller than that of light. Yet, they can interact with the sample due to their electrical charge, thus producing an image of the sample.

2.2.1. SCANNING ELECTRON MICROSCOPE (SEM).

The scanning electron microscope (SEM) is a type of electron microscope capable of producing high-resolution images of a sample surface. SEM images, due to the manner in which they are created, have a characteristic three-dimensional appearance and are useful for judging the surface structure of the sample [17].

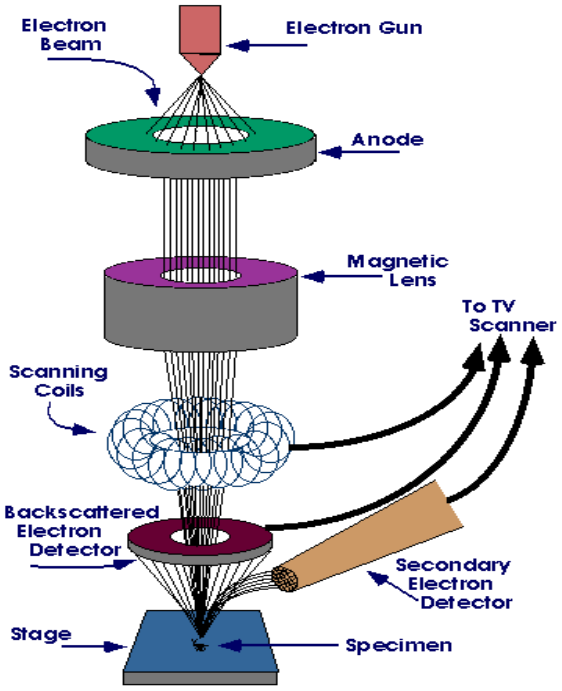

Figure 2.3 Systematic diagram of SEM

2.2.1.1. Construction and Working of SEM

Though the SEM also uses electrons to image a sample surface, the Construction and working of an SEM are different from that of the TEM.

2.2.1.2. Scanning Process

In a typical SEM, electrons are emitted thermionically or via field emission. In thermionic emission, electrons are emitted from a tungsten or lanthanum hexaboride cathode and are accelerated towards an anode. Tungsten is used because it has the highest melting point and lowest vapour pressure of all metals, thereby allowing it to be heated for electron emission. The high energy electron beam is focused, by one or two condenser lenses, into a beam with a very fine focal spot sized 1 nm to 5 nm.

Scanning coils present in the objective lens deflect the beam horizontally and vertically so that it scans a rectangular area on the sample surface in a raster fashion. On interacting with the sample, the electrons lose energy by repeated scattering and absorption within a teardrop-shaped volume of the specimen known as the interaction volume. The size of the interaction volume, which extends from less than 100 nm to around 5 µm into the surface, depends on the beam

accelerating voltage, the atomic number of the specimen and the specimen's density. The energy exchange between the electron beam and the sample results in the emission of electrons and electromagnetic radiation which can be detected to produce an image, as described below.

2.2.1.3. Detection of secondary electrons

The most common imaging mode monitors low energy (<50 eV) secondary electrons. Due to their low energy, these electrons originate within a few nanometres from the surface. The electrons are detected by a scintillator-photomultiplier device and the resulting signal is rendered into a two-dimensional intensity distribution that can be viewed and saved as a Digital image. This process relies on a raster-scanned primary beam. The brightness of the signal depends on the number of secondary electrons reaching the detector. Steep surfaces and edges tend to be brighter than flat surfaces, since the electron beam is not incident on them perpendicularly, but at an angle, causing the escape of a greater number of secondary electrons from the sample surface. This difference in brightness results in images with a well-defined, three-dimensional appearance.

2.2.1.4. Detection of backscattered electrons

Backscattered electrons consist of high-energy electrons originating in the electron beam that are reflected or back-scattered out of the specimen interaction volume. Backscattered electrons may be used to detect contrast between areas with different chemical compositions, especially when the average atomic number of the various regions is different, since the brightness of the BSE image tends to increase with the atomic number. Backscattered electrons can also be used to form electron backscatter diffraction (EBSD) image. This image can be used to determine the crystallographic structure of the specimen.

2.2.1.5. Resolution of the SEM

The spatial resolution of the SEM is limited by the size of the electron spot and the interaction volume. The spot size and the interaction volume are both very large compared to the distances between atoms. So the resolution of the SEM is not high enough to image down to the atomic scale, as is possible in the transmission electron microscope (TEM). But the SEM has compensating advantages, including the ability to image a comparatively large area of the

specimen; the ability to image bulk materials (not just thin films or foils); and the variety of analytical modes available for measuring the composition and nature of the specimen. Depending on the instrument, the resolution can fall somewhere between less than 1 nm and 20 nm. In general, SEM images are much easier to interpret than TEM images.

2.2.1.6 Equipment Details

Model	: LEO 440 PC BASED DIGITAL SEM
Resolution	: 3.5 nm SEI MODE
	: 5.5 nm BEI MODE
Signal	: SECONDARY ELECTRON
Detectors	: BACKSCATTRED ELECTRON
	CATHODOLUMINESCENCE
Magnification	: 5 X TO 300,000 X
Accelerating Voltage	: 300 V – 40 kV
Specimen Stage	: 5 - AXIS MOTORIZED
Specimen Chamber	: 27 cm x 27 cm x 25 cm
Vacuum System	: Turbo Molecular Pump
Heat and Cold Stage	: -185 to + 400^{o}C

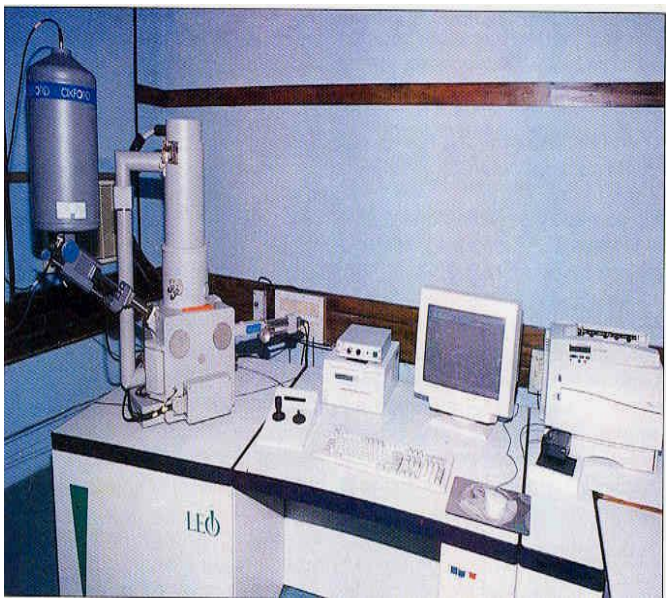

Figure 2.4 SEM Facility at NPL

2.2.2 ENERGY-DISPERSIVE X-RAYSPECTROSCOPY (EDS) Energy dispersive X-ray spectroscopy (EDS, EDX or EDXRF) is an analytical technique used for the elemental analysis or chemical characterization of a sample used in conjunction with scanning electron microscopy (SEM). The EDS technique detects x-rays emitted from the sample during bombardment by an electron beam to characterize the elemental composition of the analyzed volume.

When the sample is bombarded by the SEM's electron beam, electrons are ejected from the atoms comprising the sample's surface. The resulting electron vacancies are filled by electrons from a higher state, and an x-ray is emitted to balance the energy difference between the two electrons' states. The x-ray energy is characteristic of the element from which it was emitted.

A detector is used to convert X-ray energy into voltage signals; this information is sent to a pulse processor, which measures the signals and passes them onto an analyzer for data display and analysis. The EDS x-ray detector measures the relative abundance of emitted x-rays versus their energy. The detector is typically lithium-drifted silicon, solid-state device. When an incident x-ray strikes the detector, it creates a charge pulse that is proportional to the energy of the x-ray. The charge pulse is converted to a voltage pulse (which remains proportional to the x-ray energy) by a charge-sensitive preamplifier. The signal is then sent to a multichannel analyzer where the pulses are sorted by voltage. The energy, as determined from the voltage measurement for each incident x-ray is sent to a computer for display and further data evaluation. The spectrum of x-ray energy versus counts is evaluated to determine the elemental composition of the sampled volume.

There are four primary components of the EDS setup: the beam source; the X-ray detector; the Pulse processor; and the analyzer. Accuracy of EDS spectrum can be affected by many variants. Windows in front of the SiLi detector can absorb low-energy X-rays (i.e. EDS detectors cannot detect presence of elements with atomic number less than 5, meaning that EDS cannot detect H, He, Li, or Be). The accuracy of the spectrum can also be affected by the nature of the sample. X-rays can be generated by any atom in the sample that is sufficiently excited by the incoming beam. These X-rays are emitted in any direction, and so may not all escape the sample. The likelihood of an X-ray escaping the specimen, and thus being available to detect and measure depends on the energy of the X-ray and the amount and density of material it has to pass through. This can result in reduced accuracy in inhomogeneous and rough samples.

Now there is a trend towards a newer EDS detector, called the Silicon Drift Detector (SDD). The SDD consists of a high-resistivity silicon chip where electrons are driven to a small collecting anode. The advantage lies in the extremely low capacitance of this anode, thereby utilizing shorter processing times and allowing very high throughput. Benefits of the SDD include 1) High count rates and processing 2) Better resolution than traditional SiLi detectors at high count rates 3) Lower dead time (time spent on processing x-ray event) 4) Faster analytical capabilities and more precise X-ray maps or particle data collected in seconds and 5) Ability to be stored and operate at relatively high temperatures, eliminating the need for liquid nitrogen cooling.

2.2.2.1 ANALYTICAL INFORMATION

Qualitative Analysis – The sample x-ray energy values from the EDS spectrum are compared with known characteristic x-ray energy values to determine the presence of an element in the sample. Elements with atomic numbers ranging from that of beryllium to uranium can be detected. The minimum detection limits vary from approximately 0.1 to a few atom percent, depending on the element and the sample matrix.

Quantitative Analysis – Quantitative results can be obtained from the relative x-ray counts at the characteristic energylevels for the sample constituents. Semi-quantitative results are readily available without standards by using mathematical corrections based on the analysis parameters and the sample composition. The accuracy of standardless analysis depends on the sample composition. Greater accuracy is obtained using known standards with similar structure and composition to that of the unknown sample.

2.2.2.2 TYPICAL APPLICATIONS

• Foreign material analysis
• Corrosion evaluation

• Coating composition analysis
• Rapid material alloy identification
• Small component material analysis
• Phase identification and distribution

2.2.3 HIGH RESOLUTION TRANSMISSION ELECTRON MICROSCOPE [HRTEM].

Transmission electron microscopy (TEM) is an imaging technique whereby a beam of electrons is transmitted through a specimen, then an image is formed, magnified and directed to appear either on a fluorescent screen or layer of photographic film (see electron microscope), or to be detected by a sensor such as a CCD camera[18,19].

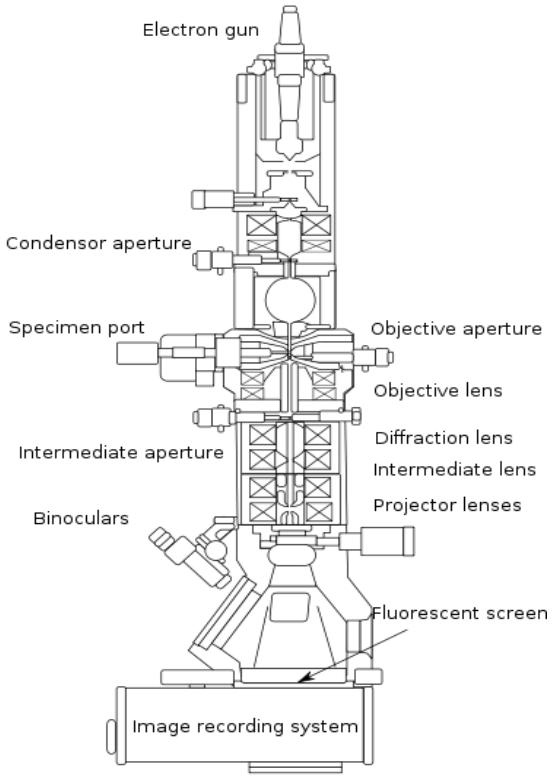

Figure 2.5 Systematic diagram of HRTEM

2.2.3.1. The Setup: The following are the major components of a TEM.

2.2.3.2 Electron gun: The electrons are generated and accelerated to the required high energy.

2.2.3.3 Condenser system: A set-up of different magnetic lenses and apertures makes it possible to get either a parallel beam (micro probe for TEM) or a convergent beam with selected

convergence angles (nano probe for STEM and CBED). Furthermore, the beam can be scanned (STEM) or tilted (DF-TEM).

2.2.3.4 Objective lens: Most important lens in the microscope since it generates the first intermediate image, the quality of which determines the resolution of the final image.

2.2.3.5 Diffraction/intermediate lens: Switching between imaging and diffraction mode.

2.2.3.6 Projective lenses: Further magnification of second intermediate image (image or diffraction pattern, respectively).

Image observation: Images and diffraction pattern can directly be observed on the viewing screen in the projection chamber or via a TV camera mounted below the microscope column. Images can be recorded on negative films, on slow-scan CCD cameras or on imaging plates.

Vacuum system: Because of strong interactions of electron with matter, gas particles must be absent in the column. The required high vacuum is maintained by a vacuum system typically comprising a rotary pump (pre-vacuum pump), a diffusion pump and one or more ion getter pumps.

2.2.3.7 The Working

1. The Electrons are generated by a process known as thermionic discharge in the same manner as the cathode in a cathode ray tube, or by field emission.
2. The electrons are then accelerated by an electric field and focused by electrical and magnetic fields, called condenser lenses, onto the sample.
3. The beam is restricted by the condenser to knock out the high angle electrons, that are far from the optic axis of the microscope.
4. When the beam strikes the sample, portions of it are transmitted, deflected and absorbed. The amount of absorption is very little.
5. The transmitted portion is focused by the objective lens into an image
6. The objective aperture enhances the contrast of the image by blocking out high-angle diffracted electrons.
7. The image is enlarged while it is being passed down the column through immediate and projector lenses.
8. The image strikes the phosphor image screen and light is generated, allowing the user to see the image. The darker areas of the image represent those areas of the sample that

fewer electrons were transmitted through. The lighter areas of the image represent those areas of the sample that more electrons were transmitted through.

2.2.3.8 Equipment Details

Model	: FEI-Tecnai F30 G^2 STWIN (300kV FEG)
TEM Point Resolution	: 0.205 nm
TEM Line Resolution	: 0.144 nm
STEM resolution	: 0.17 nm
EDAX resolution	: 136 eV
Accelerating voltage	: 80, 100, 120, 160, 200 KV
Specimen heating	: UP TO 1000^{O} C

Figure 2.6 HRTEM at NPL

2.3 Electron Paramagnetic Resonance(EPR):

spectroscopy is a technique for studying chemical species that have one or more unpaired electrons, such as organic and inorganic free radicals or inorganic complexes possessing a transition metal ion. The basic physical concepts of EPR are analogous to those of nuclear magnetic resonance (NMR), but it is electron spins that are excited instead of spins of atomic nuclei. Because most stable molecules have all their electrons paired, the EPR technique is less widely used than NMR. However, this limitation to paramagnetic species also means that the EPR technique is one of great specificity, since ordinary chemical solvents and matrices do not give rise to EPR spectra.

EPR was first observed in Kazan State University by Soviet physicist Yevgeny Zavoisky in 1944, and was developed independently at the same time by Brebis Bleaney at the University of Oxford.

Figure 2.7 EPR machine at NPL

2.3.1 Origin of an EPR signal

Every electron has a magnetic moment and spin quantum number s = 1/2, with magnetic components $m_s = +1/2$ and $m_s = -1/2$. In the presence of an external magnetic field with strength B_0, the electron's magnetic moment aligns itself either parallel ($m_s = -1/2$) or antiparallel ($m_s =$

+1/2) to the field, each alignment having a specific energy (see the Zeeman effect). The parallel alignment corresponds to the lower energy state, and the separation between it and the upper state is $\Delta E = g_e \mu_B B_0$, where g_e is the electron's so-called g-factor (see also the Landé *g*-factor) and μ_B is the Bohr magneton. This equation implies that the splitting of the energy levels is directly proportional to the magnetic field's strength, as shown in the diagram below.

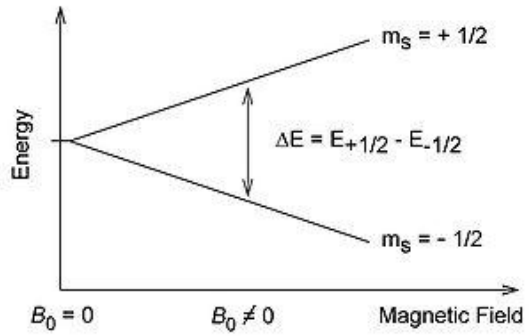

An unpaired electron can move between the two energy levels by either absorbing or emitting electromagnetic radiation of energy $\varepsilon = h\nu$ such that the resonance condition, $\varepsilon = \Delta E$, is obeyed. Substituting in $\varepsilon = h\nu$ and $\Delta E = g_e \mu_B B_0$ leads to the fundamental equation of EPR spectroscopy: $h\nu = g_e \mu_B B_0$. Experimentally, this equation permits a large combination of frequency and magnetic field values, but the great majority of EPR measurements are made with microwaves in the 9000–10000 MHz (9–10 GHz) region, with fields corresponding to about 3500 G (0.35 T). See below for other field-frequency combinations.

In principle, EPR spectra can be generated by either varying the photon frequency incident on a sample while holding the magnetic field constant, or doing the reverse. In practice, it is usually the frequency which is kept fixed. A collection of paramagnetic centers, such as free radicals, is exposed to microwaves at a fixed frequency. By increasing an external magnetic field, the gap between the $m_s = +1/2$ and $m_s = -1/2$ energy states is widened until it matches the energy of the microwaves, as represented by the double-arrow in the diagram above. At this point the unpaired electrons can move between their two spin states. Since there typically are more electrons in the lower state, due to the Maxwell-Boltzmann distribution (see below), there is a net absorption of energy, and it is this absorption which is monitored and converted into a spectrum.

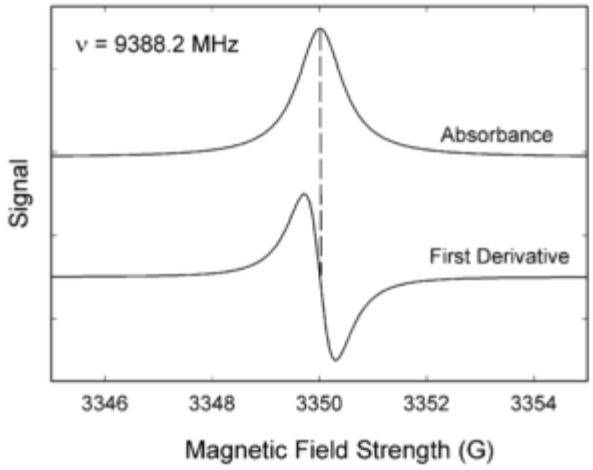

As an example of how $h\nu = g_e\mu_B B_0$ can be used, consider the case of a free electron, which has g_e = 2.0023,[20]and the simulated spectrum shown at the right in two different forms. For the microwave frequency of 9388.2 MHz, the predicted resonance position is a magnetic field of about $B_0 = h\nu / g_e\mu_B$ = 0.3350 tesla = 3350 gauss, as shown. Note that while two forms of the same spectrum are presented in the figure, most EPR spectra are recorded and published only as first derivatives.

Because of electron-nuclear mass differences, the magnetic moment of an electron is substantially larger than the corresponding quantity for any nucleus, so that a much higher electromagnetic frequency is needed to bring about a spin resonance with an electron than with a nucleus, at identical magnetic field strengths. For example, for the field of 3350 G shown at the right, spin resonance occurs near 9388.2 MHz for an electron compared to only about 14.3 MHz for ^{1}H nuclei. (For NMR spectroscopy, the corresponding resonance equation is $h\nu = g_N\mu_N B_0$ where g_N and μ_N depend on the nucleus under study.)

2.3.2 Maxwell-Boltzmann distribution

In practice, EPR samples consist of collections of many paramagnetic species, and not single isolated paramagnetic centers. If the population of radicals is in thermodynamic equilibrium, its statistical distribution is described by the Maxwell-Boltzmann equation

$$\frac{n_{\text{upper}}}{n_{\text{lower}}} = \exp\left(-\frac{E_{\text{upper}} - E_{\text{lower}}}{kT}\right) = \exp\left(-\frac{\Delta E}{kT}\right) = \exp\left(-\frac{\epsilon}{kT}\right) = \exp\left(-\frac{h\nu}{kT}\right)$$

where n_{upper} is the number of paramagnetic centers occupying the upper energy state, k is the Boltzmann constant, and T is the temperature in kelvins. At 298 K, X-band microwave frequencies ($\nu \approx 9.75$ GHz) give $n_{upper} / n_{lower} \approx 0.998$, meaning that the upper energy level has a smaller population than the lower one. Therefore, transitions from the lower to the higher level are more probable than the reverse, which is why there is a net absorption of energy.

The sensitivity of the EPR method (i.e., the minimum number of detectable spins N_{min}) depends on the photon frequency ν according to

$$N_{\mathrm{min}} = \frac{k_1 V}{Q_0 k_f \nu^2 P^{1/2}}$$

where k_1 is a constant, V is the sample's volume, Q_0 is the unloaded quality factor of the microwave cavity (sample chamber), k_f is the cavity filling coefficient, and P is the microwave power in the spectrometer cavity. With k_f and P being constants, $N_{min} \sim (Q_0 \nu^2)^{-1}$, i.e., $N_{min} \sim \nu^{-\alpha}$, where $\alpha \approx 1.5$. In practice, α can change varying from 0.5 to 4.5 depending on spectrometer characteristics, resonance conditions, and sample size. In other words, the higher the spectrometer frequency the lower the detection limit (N_{min}), meaning greater sensitivity.

2.3.3 Spectral parameters

In real systems, electrons are normally not solitary, but are associated with one or more atoms. There are several important consequences of this:

1. An unpaired electron can gain or lose angular momentum, which can change the value of its g-factor, causing it to differ from g_e. This is especially significant for chemical systems with transition-metal ions.
2. If an atom with which an unpaired electron is associated has a non-zero nuclear spin, then its magnetic moment will affect the electron. This leads to the phenomenon of hyperfine coupling, analogous to J-coupling in NMR, splitting the EPR resonance signal into doublets, triplets and so forth.

3. Interactions of an unpaired electron with its environment influence the shape of an EPR spectral line. Line shapes can yield information about, for example, rates of chemical reactions.
4. The *g*-factor and hyperfine coupling in an atom or molecule may not be the same for all orientations of an unpaired electron in an external magnetic field. This anisotropy depends upon the electronic structure of the atom or molecule (e.g., free radical) in question, and so can provide information about the atomic or molecular orbital containing the unpaired electron.

2.3.4 The *g* factor

Knowledge of the *g*-factor can give information about a paramagnetic center's electronic structure. An unpaired electron responds not only to a spectrometer's applied magnetic field B_0, but also to any local magnetic fields of atoms or molecules. The effective field B_{eff} experienced by an electron is thus written

$$B_{\text{eff}} = B_0(1 - \sigma)$$

where σ includes the effects of local fields (σ can be positive or negative). Therefore, the $h\nu = g_e\mu_B B_{eff}$ resonance condition (above) is rewritten as follows:

$$h\nu = g_{\text{e}}\mu_B B_{\text{eff}} = g_{\text{e}}\mu_B B_0(1 - \sigma)$$

The quantity $g_e(1 - \sigma)$ is denoted g and called simply the *g*-factor, so that the final resonance equation becomes

$$h\nu = g\mu_B B_0$$

This last equation is used to determine g in an EPR experiment by measuring the field and the frequency at which resonance occurs. If g does not equal g_e the implication is that the ratio of the unpaired electron's spin magnetic moment to its angular momentum differs from the free electron value. Since an electron's spin magnetic moment is constant (approximately the Bohr magneton),

then the electron must have gained or lost angular momentum through spin-orbit coupling. Because the mechanisms of spin-orbit coupling are well understood, the magnitude of the change gives information about the nature of the atomic or molecular orbital containing the unpaired electron.

2.3.5 Resonance linewidth definition

Resonance linewidths are defined in terms of the magnetic induction *B*, and its corresponding units, and are measured along the *x* axis of an EPR spectrum, from a line's center to a chosen reference point of the line. These defined widths are called half widths and possess some advantages: for asymmetric lines values of left and right halfwidth can be given. The half width ΔB_h is the distance measured from the line's center to the point in which absorption value has half of maximal absorption value in the center of resonance line. First inclination width $\Delta B_{1/2}$ is a distance from center of the line to the point of maximal absorption curve inclination. In practice, a full definition of line width is used. For symmetric lines, half width $\Delta B_{1/2} = 2\Delta B_h$, and full inclination width $\Delta B_{max} = 2\Delta B_{1s}$

Applications

EPR spectroscopy is used in various branches of science, such as chemistry and physics, for the detection and identification of free radicals and paramagnetic centers such as F centers. EPR is a sensitive, specific method for studying both radicals formed in chemical reactions and the reactions themselves. For example, when frozen water (solid H_2O) is decomposed by exposure to high-energy radiation, radicals such as H, OH, and HO_2 are produced. Such radicals can be identified and studied by EPR. Organic and inorganic radicals can be detected in electrochemical systems and in materials exposed to UV light. In many cases, the reactions to make the radicals and the subsequent reactions of the radicals are of interest, while in other cases EPR is used to provide information on a radical's geometry and the orbital of the unpaired electron.

Medical and biological applications of EPR also exist. Although radicals are very reactive, and so do not normally occur in high concentrations in biology, special reagents have been developed to spin-label molecules of interest. These reagents are particularly useful in biological systems.

Specially-designed nonreactive radical molecules can attach to specific sites in a biological cell, and EPR spectra can then give information on the environment of these so-called spin-label or spin-probes.

A type of dosimetry system has been designed for reference standards and routine use in medicine, based on EPR signals of radicals from irradiated polycrystalline α-alanine(the alanine deamination radical, the hydrogen abstraction radical, and the $(CO^{-}(OH))=C(CH_3)NH_2^{+}$ radical) . This method is suitable for measuring gamma and x-rays, electrons, protons, and high-linear energy transfer (LET) radiation of doses in the 1 Gy to 100 kGy range.[22]

EPR spectroscopy can only be applied to systems in which the balance between radical decay and radical formation keeps the free-radicals concentration above the detection limit of the spectrometer used. This can be a particularly severe problem in studying reactions in liquids. An alternative approach is to slow down reactions by studying samples held at cryogenic temperatures, such as 77 K (liquid nitrogen) or 4.2 K (liquid helium). An example of this work is the study of radical reactions in single crystals of amino acids exposed to x-rays, work that sometimes leads to activation energies and rate constants for radical reactions.

The study of radiation-induced free radicals in biological substances (for cancer research) poses the additional problem that tissue contains water, and water (due to its electric dipole moment) has a strong absorption band in the microwave region used in EPR spectrometers.

EPR also has been used by archaeologists for the dating of teeth. Radiation damage over long periods of time creates free radicals in tooth enamel, which can then be examined by EPR and, after proper calibration, dated. Alternatively, material extracted from the teeth of people during dental procedures can be used to quantify their cumulative exposure to ionizing radiation. People exposed to radiation from the Chernobyl disaster have been examined by this method.[23,24]

Radiation-sterilized foods have been examined with EPR spectroscopy, the aim being to develop methods to determine if a particular food sample has been irradiated and to what dose.

Because of its high sensitivity, EPR was used recently to measure the quantity of energy used locally during a mechanochemical milling process.[25]

EPR spectroscopy has been used to measure properties of crude oil, in particular asphaltene and vanadium content. EPR measurement of asphaltene content is a function of spin density and solvent polarity. Prior work dating to the 1960s has demonstrated the ability to measure vanadium content to sub-ppm levels.

2.4 Physical Property Measurment System (PPMS):

The PPMS is an automated low-temperature and magnet system for the measurement of material properties like specific heat, magnetic AC and DC susceptibility and both electrical and thermal transport properties. The base unit of the PPMS consists of a cryostat with a superconducting magnet coil. The different measurement possibilities (options) result from the use of different measurement inserts or sample holders and the call of the according software mode. The optional modern version features an integrated Helium-Reliquefier which makes the system virtually cryogen-free. Only Helium-gas is needed for purging the sample chamber.

2.4.1 Features of PPMS

Fully-automated variable temperature and magnetic field system with multiple measurement applications:

– Thermal transport and heat capacity

– DC magnetometry and AC susceptibility

– Electro-transport

Multi-function probe with integrated sample platforms (“pucks”) using plug-in technology

– Temperature control from 0.35 K - 400 K

Temperature range varies for each option

– 9 Tesla longitudinal magnet

– < 10-4 Torr high vacuum available

– 30 kbar pressure cell for electrical measurements

2.4.2 PPMS FOR MAGNETIZATION

• Measures AC susceptibility: $\chi = dM/dH$, and DC magnetization: $M = M(H,T)$

• AC susceptibility sensitivity: 5x10-8 emu @ 10 kHz

• DC magnetization measured with the extraction method: extraction speed: 100 cm s-1; sensitivity of 2x10-5 emu

- 1 -10f harmonics calculated (software selectable)

– AC Frequency Range: 10 Hz to 10 kHz

• At low temperatures the range depends on the frequency and duration of the measurement

– Temperature Range: 1.9 K - 350 K

– Magnetic field range: ± 9 Tesla

2.4.3 Advantages of PPMS

• Very low minimum temperature (0.35 K) with the 3He option

• Fast measurement times: up to 12 K/min slew rates

• Custom designed experiments

• Measure several physical properties at once, e.g.:

– Electrical conductivity, thermal conductivity

– Magnetic susceptibility, magnetization

– Magnetic dependence of heat capacity

– Effects of pressure on electrical properties

• Small sample sizes (typically 10 to 100 mg)

• EverCool Dewar with very low He loss

2.5. Vibrating Sample Magnetometer (VSM):

The VMS, first developed by Foner in the late 1950s, is a basic research tool for determining magnetic properties in a variety of studies of the structure of paramagnetic, ferromagnetic, antiferromagnetic, diamagnetic and ferrimagnetic materials. If any material is placed in a uniform magnetic field, a dipole moment will be induced in the sample proportional to the product of the sample susceptibility and the applied field. If the sample is made to undergo sinusoidal motion, the resulting magnetic flux changes

near the sample will induce an electrical signal in suitably placed stationary coils. This signal will be proportional to the moment, amplitude, and frequency of vibration.

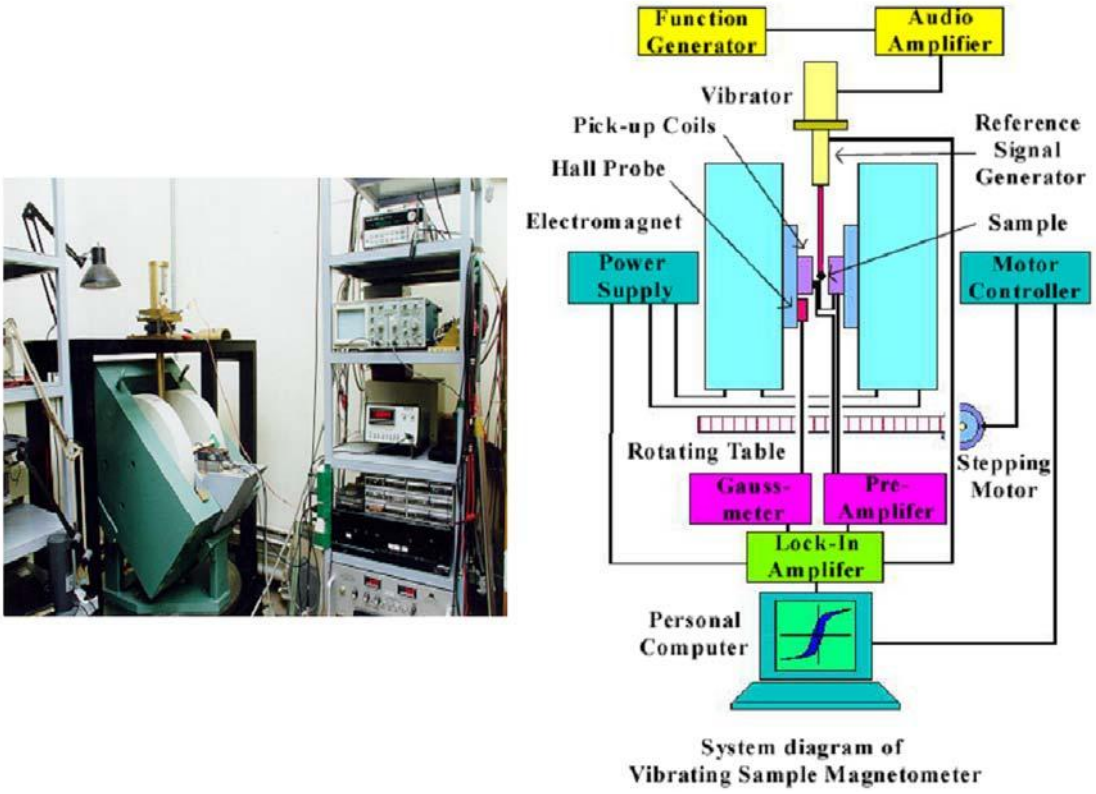

Figure 2.8 The actual photograph of VSM instrument along with the pictorial

Figure 2.8 shows a typical VSM setup. The material under study in the VSM is inserted in the sample holder so that it rests centered in a pair of pickup coils between the poles of an electro magnet. The sample holder is mounted using a sample rod in a ransducer assembly, which passes through the center of a driving coil. The transducer is driven by a power amplifier which itself is driven by an oscillator. The magnetic sample under study is constraint to vibrate only along the vertical axis. As it does so, it induces a signal in the sample pickup coils as described above. The magnitude of this signal is dependent on the magnetic properties of the sample itself. Attached to the sample holder rod is a permanent magnet.

A pair of stationary coils pick up the induced ac signal, which is proportional to the amplitude and frequency of the vibration and is used as a control signal for modulation of the transducer.The output of the sample coil is fed to the differential input of a lock-in amplifier. The reference input of the lock-in comes from the sine wave oscillator used to drive the sample holder. The output of the lock-in goes to the data acquisition computer as well as the magnitude of the applied magnetic field coming from a gaussmeter. The signal from the lock-in amplifier is directly proportional to the magnetic moment of the sample. The computer is now able to graph the magnetic moment of the sample against the applied magnetic field.

CHAPTER 3

EXPERIMENTAL

3.1 Synthesis of FePt Nanoparticle:

3.1.1 SUPERHYDRIDE REDUCTION OF $FeCl_2$ AND $Pt(acac)_2$ AT HIGH TEMPERATURE.

3.1.1.1 CHEMICALS

The synthesis was carried out using standard airless procedures and commercially available reagents. Absolute ethanol (EtOH), hexane (C_6H_{14}), Sodium borohydride ($NaBH_4$)**,** 1,2-hexadecanediol **(**$CH_3(CH_2)_{13}CH(OH)CH_2OH$**)**, oleic acid **(**$C_{17}H_{33}COOH$**)**, Iron (II) chloride tetrahydrate ($FeCl_2.4H_2O$), Oleylamine **(**$CH_3(CH_2)_7CH{=}CH(CH_2)_8NH_2$**)** were purchased from Aldrich Chemical Co. Di-phenyl ether **(**$O(C_6H_5)_2$**),** polyethylenimine **(**$(\text{-}NHCH_2CH_2\text{-})_X(N(CH_2CH_2NH_2)H_2CH_2\text{-})_Y$**)**, Platinum acetylacetonate **(**$Pt(acac)_2$**)**, and Dichlorobenzene (DCB)**(**($C_6H_4Cl_2$**)**, was from Alfa Aesar Co.

3.1.1.2 EXPERIMENTAL SET UP

A Special Teflon coated heating plate with temperature sensor and magnetic stirrer, three mouth round bottom flask, Nitrogen gas cylinder, A condenser unit, Clamp stand.

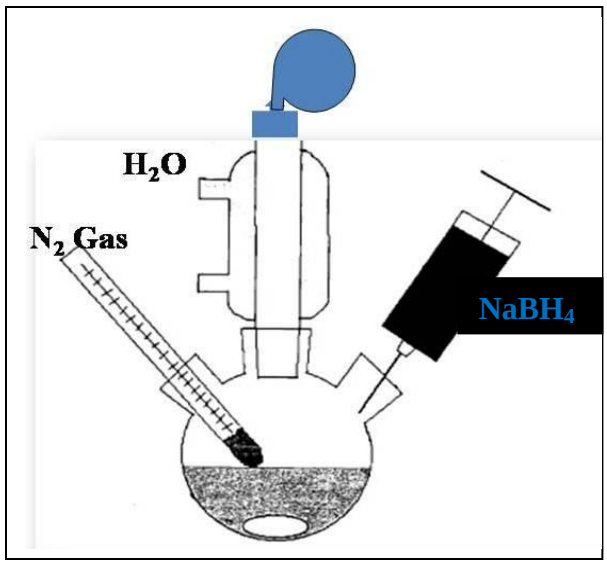

Figure 3.1 Experimental set up

3.1.1.3 EXPERIMENTAL

$Pt(acac)_2$ (49.25 mg), $FeCl_2.4H_2O$ (34.75 mg), 1,2-hexadecanediol (130 mg), and Di-phenyl ether (25 mL) is added under nitrogen atmosphere, into a flask equipped with a N_2 in/outlet, septa rubber, and a thermal probe.The mixture is heated to 100 °C for 10 min. Then Oleic acid (0.4 ml) and oleylamine (0.4 ml) are added, and the mixture is continuously heated to 200 °C for 20 min.

2.5 ml of $NaBH_4$ (1 M DCB solution) is slowly injected into the mixture over a duration of 2 min. The black dispersion is stirred at 200 °C for 5 min under N_2 to remove low boiling solvent and under a blanket of N_2 solution is heated to reflux at 263 °C for 20 min. The heating source is now removed, and the black reaction mixture is cooled to room temperature.

Ethanol (40 ml) is then added. The black product is precipitated and separated by centrifugation (6000 rpm, 10 min).The yellow-brown supernatant is discarded and the black product is dispersed in hexane (20 ml) in the presence of oleic acid (0.05 ml) and oleylamine (0.02 ml). Any undissolved material is removed by centrifugation (6000 rpm, 10 min). The product is then precipitated out by adding ethanol (20 ml) and separated with centrifugation (6000 rpm, 10 min). It is once again dispersed in hexane in the presence of oleic acid and oleylamine, precipitated out by adding ethanol and separated with centrifugation. The product, FePt nanoparticles, is re-dispersed in hexane solvent for further use.

3.1.2 SYNTHESIS BY AQUEOUS ROUTE.

3.1.2.1 CHEMICALS

The synthesis is carried out using commercially available reagents. Absolute ethanol (EtOH), hexane(C_6H_{14}), Chloroplatinic Acid hydrate($H_2PtCl_6.H_2O$), Ferrus chloride($FeCl_2x4H_2O$), sodium dodecylsulfate(SDS)**(**$CH_3(CH_2)_{11}OSO_3Na$**)**, hydrazine (N_2H_4) were purchased from Aldrich Chemical Co.

3.1.2.2 EXPERIMENTAL SET UP

A Special Teflon coated heating plate with temperature sensor and magnetic stirrer, round bottom flask, Clamp stand.

3.1.2.3 EXPERIMENTAL

$4x10^{-4}$ mol of $H_2PtCl_6.H_2O$, $4x10^{-4}$ mol of $FeCl_2.4H_2O$, and $8x10^{-4}$ mol of a surfactant are dissolved into 20 ml of distilled water. Sodium dodecylsulfate (SDS) is used as surfactant. The salt/surfactant solution is homogenized and 20 ml of an aqueous solution of hydrazine (N_2H_4; $8x10^{-3}$ mol) is injected under vigorous stirring. The solution colour immediately turned to black indicating reduction. The system is heated to 70 ^oC for 3 h, then cooled down to room temperature.

The black product is precipitated by adding 20 ml of EtOH and isolated after centrifugation. The solid is redispersed in hexane or washed twice with EtOH and dried under N_2 for 24h.

3.2 FePt Nanoparticle Asembly:

3.2.1 METHODOLOGY

As synthesized FePt nanoparticles powde was used to form a thin film in the presence of polyethylenimine (PEI). Thin film of FePt nanoparticles on a silicon substrate facilitates to anneal the particles at high temperature without much agglomeration, for this purpose we need polyethylenimine (PEI), a branched polymer.

A naturally oxidized silicon substrate is cleaned using ethanol and dried under a flow of N_2.The substrate is then immersed into the chloroform solution of PEI (20 mg/mL) for about 30 s, withdrawn from the solution and dipped into ethanol solvent to wash off extra PEI on the substrate surface and dried.

The PEI functionalized substrate is immersed into the hexane dispersion of FePt nanoparticles (10 mg/mL) for 30 s, withdrawn from the dispersion, rinsed with fresh hexane, and

dried. This yielded one layer of PEI/FePt assembly. By repeating the coating of PEI and FePt, the multilayer of 4 nm FePt nanoparticle assembly is easily made.

3.2.2 THERMAL ANNEALING

The PEI/FePt assemblies are thermally annealed for further characterization. The annealing transforms the particle structure from the chemically disordered fcc phase to the chemically ordered fct phase, rendering FePt nanoparticles with desirable high magnetocrystalline anisotropy and ferromagnetism at room temperature.

Further, the annealing also results in the decomposition of the PEI and oleic acid/oleylamine left around FePt particles into carbonaceous matrix, yielding smooth FePt nanoparticle assemblies. The annealing is performed in an inert atmosphere (N_2 or He) in a quartz tube at temperatures ranging from 400 to 800 °C and durations between 2 min and 2 h.

CHAPTER 4

RESULTS AND DISCUSSION

4.1 Superhydride Reduction of $FeCl_2$ and $Pt(acac)_2$ at high temp:

The reduction of $FeCl_2$ and $Pt(acac)_2$ mixture by superhydride in the presence of oleic acid, oleylamine, and 1,2-hexadecanediol at 200 °C, followed by refluxing at 263 °C, led to monodisperse 2 nm FePt nanoparticles. Although the reduction is usually performed at 200 °C, experimental results show that superhydride could be added at any temperature in the range between 200 and 263 °C. Adding the reducing agent at lower temperature (<200 °C) did not yield high quality FePt nanoparticle materials.

Two metal precursors, $FeCl_2$ and $Pt(acac)_2$, are specifically chosen for this reduction process as they formed clear Di-phenyl ether solution when mixed. Presumably, the mixing of $FeCl_2$ and $Pt(acac)_2$ resulted in an $FeCl_2$-$Pt(acac)_2$ intermediate that facilitated the formation of FePt nanoparticles under the current reaction condition. The $FeCl_2$ used in the reaction can be in either anhydrous state or hydrated state. If $FeCl_2.4H_2O$ is used, the mixture is usually stirred at 200 °C under nitrogen for about 20 min before the reducing agent, superhydride, is added to the mixture.

Several different reducing agents have been tested for the reduction process. Metal naphthalides are very powerful reducing agents but are also difficult to store because of their extremely air- and moisture-sensitive nature. Polyalcohols, such as ethylene glycol and 1,2-hexanedecanediol, or other long chain alkyl alcohols are not a strong reducing agent for the $FeCl_2$- $Pt(acac)_2$ reduction. However the alkyl alcohol can act like a cosurfactant and help to generate FePt nanoparticles with better quality.

Metal borohydrides are a class of well-known reducing agents for the reduction of various metal salts to metal nanoparticles.[26,29] Specifically, a borohydride derivative, such as

superhydride, $NaBH_4$, is easily dissolved in organic ether solvent, facilitating homogeneous reduction of metal salt and formation of metal nanoparticles.[30,33]

The advantages of choosing $NaBH_4$ over other metal borohydrides are as follows: (i) The Na+ cation from the superhydride can combine with Cl- or acac- from $FeCl_2$ and $Pt(acac)_2$ to form Na salt that is easily washed off from the product with alcohol; (ii) After reduction, B is usually released from the mixture: it may be removed from the system under nitrogen, or it can combine with other organic ether/amine/alcohol species in the mixture, to form organic adducts, leading to pure FePt nanoparticles.

The binary FePt nanoparticles are stabilized by oleic acid and oleylamine as in the previous decomposition/reduction process. If the final product is Fe-rich, then a combination of oleic acid/oleylamine in a ratio of >1 is needed for particle stabilization during the purification process. If the final product is Pt-rich, then a combination of oleic acid/oleylamine with the ratio of <1 is required for the stabilization. This corresponds to the fact that Fe tends to bind to -OOC while Pt to $-NH_2$.

Under the current reaction condition, the particle growth is self-limited. The size of the particles is independent of the amount of stabilizers present, the addition rate of reducing agent, the reduction temperature (from 200 °C to 263 °C), and the refluxing time (from 30 min to 2 h). 2 nm FePt particles are always separated. Refluxing may not be necessary, but it did help to yield FePt nanoparticles with better shape.

Figure 4.1 shows the TEM micrograph of **2 nm** FePt nanoparticles deposited on an amorphous carbon copper grid from their hexane dispersion. It can be seen that FePt nanoparticles are uniform with narrow size distribution.

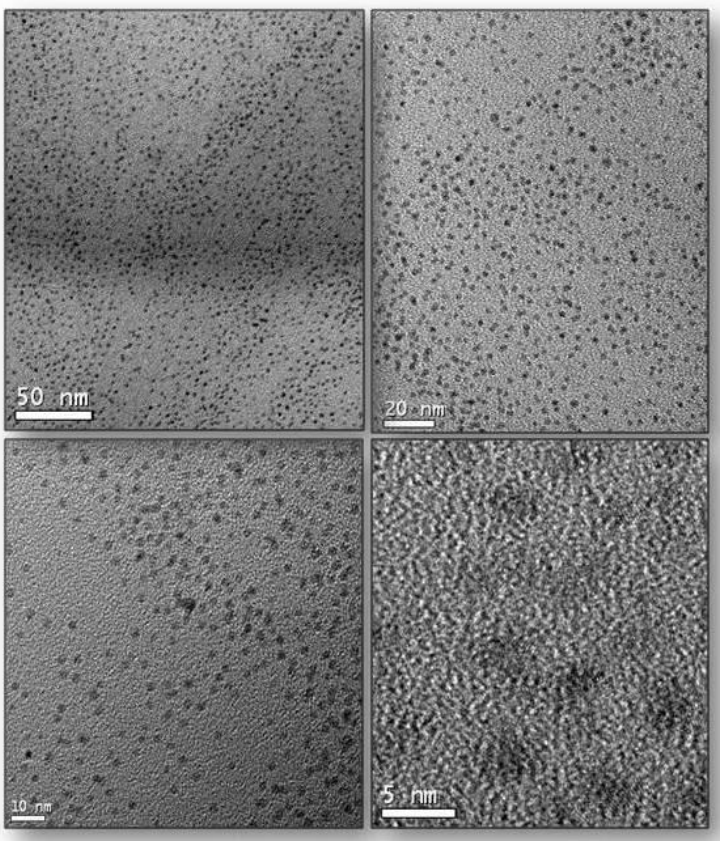

FIGURE 4.1 TEM Micrograph of FePt nanoparticle synthesized by reduction of superhydride.

4.1.1 STRUCTURAL ANALYSIS OF THE FePt NANOPARTICLE

The crystal structure of the FePt nanoparticles in a thin assembly was determined by the X-ray diffraction (XRD). The XRD of the as-synthesized FePt particles reveals a typical chemically disordered fcc structure,[34] in which Fe atoms are substituted into Pt positions and vice versa. Annealing induces the Fe and Pt atoms to rearrange into the long range chemically ordered fct structure, which can be viewed as a natural superlattice of alternating Fe and Pt atomic planes. The change of the internal particle structure upon annealing depends on annealing temperature and duration, as well as the Fe/Pt ratio. The onset of this phase change occurs at about 600 °C, which is consistent with the previous observation on FePt nanoparticles prepared from the decomposition/reduction process.[34,35,36] **Figure 4.2** shows the in-plane X-ray diffraction scans for the as-synthesized FePt nanoparticle.

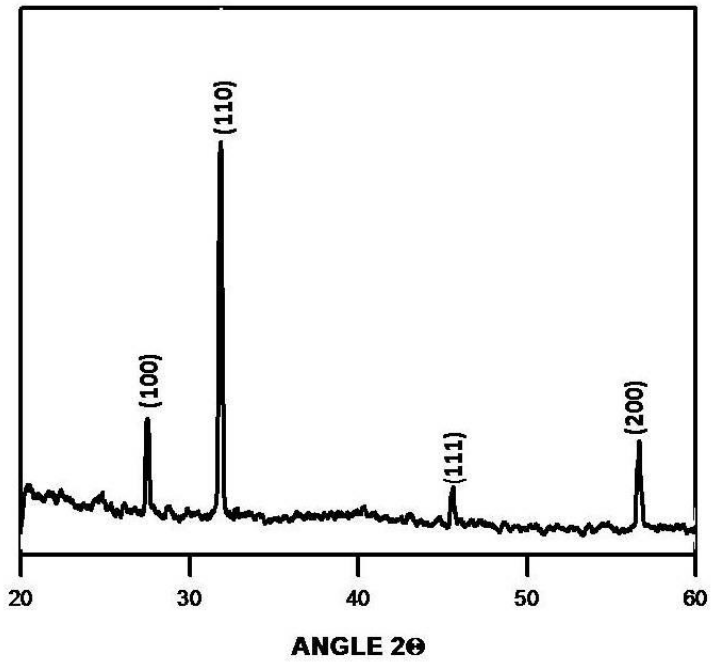

Figure 4.2 XRD of as synthesized FePt nanoparticle by superhydride reduction at high temperature.

4.1.2 MAGNETIC PROPERTIES OF THE NANOPARTICLE

Along with the structural change, magnetic properties of the assemblies can be easily tuned. The as-synthesized FePt nanoparticles have chemically disordered fcc structure, and the related thin assemblies are superparamagnetic at room temperature with *H*c=0. The thermal annealing transforms the chemically disordered fcc structure to the chemically ordered fct structure, yielding ferromagnetic thin FePt nanoparticle assemblies. The coercivity of the annealed thin films increases with annealing time and temperature, and a minimum annealing temperature of about 600 °C under an inert atmosphere is required to form ferromagnetic thin films. This corresponds to the structure transformation from the fcc phase to the fct phase at this temperature.

On the other hand, the coercivity of the annealed thin films is also found to depend on the assembly thickness. **Figure 4.3 (A)** shows the hysteresis loops as synthesized 2 nm FePt nanoparticle through PPMS at 100 K. **Figure 4.3 (B)** shows magnified image of figure 4.3(A) which shows that this nanoparticle has coercivity and remanence which is nearly 87Oe and 6 emu respectively.

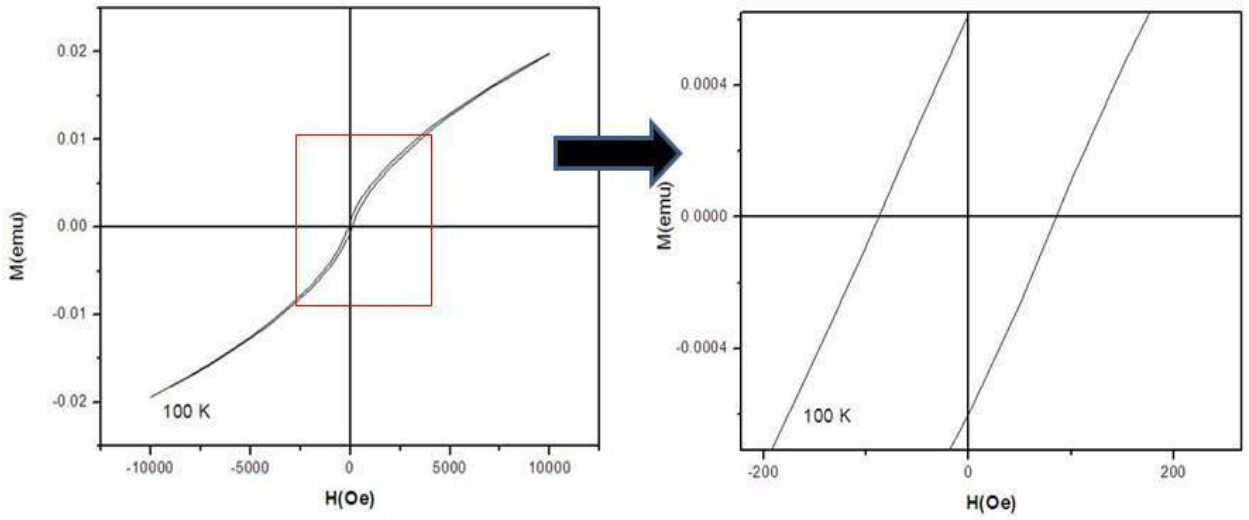

(A) **(B)**

Figure 4.3 Shows PPMS result of FePt nanoparticle made by super hydride reduction at high temperature **(A)** M-H Graph of FePt nanoparticle **(B)** Magnified image of figure 4.3 (A) to show coercivity and remanence.

The superparamagnetic behavior is may be due to the reseaon that thermal energy can overcome the anisotropy energy barrier of the individual particles, and the net magnetization of the particle assemblies is zero in the absence of an external field.

However, high-temperature annealing also results in serious particle aggregation and exchange-coupling among the neighboring particles.[39] Further experiments on controlled reductive annealing and its application in fabricating thin FePt assemblies with large Hc are underway.

4.2 SYNTHESIS IN AQUEOUS MEDIUM:

Aqueous medium synthesis is simple and safe method for FePt nanoparticles, because of it's low temperature synthesis.

TEM images show **(Figure 4.4)** deposits made up of well-dispersed particles of size 2–3 nm.

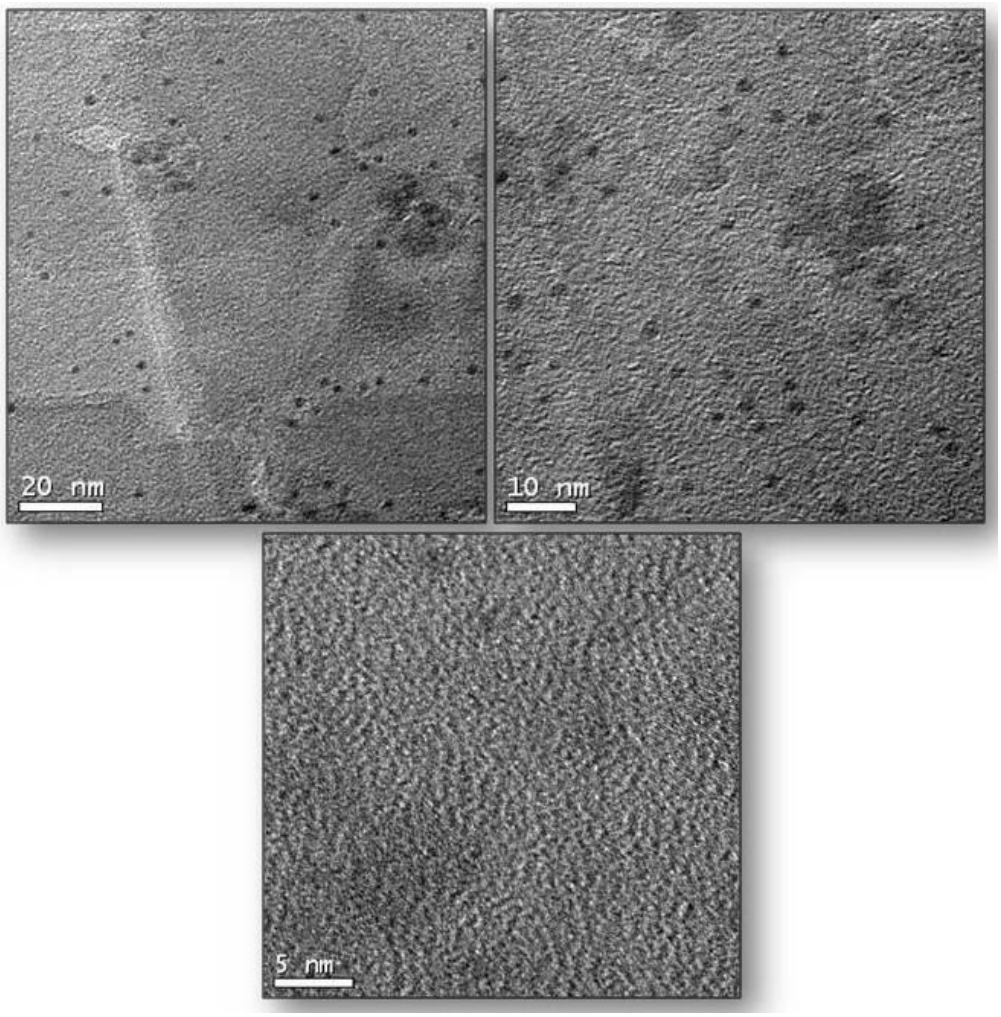

FIGURE 4.4 TEM Micrograph of FePt nanoparticle synthesized in presence of SDS as a surfactant.

4.2.1 STRUCTURAL ANALYSIS OF NANOPARTICLES

The as-made alloy nanoparticles possess an fcc structure shown by XRD graph **Figure 4.5**. Here peak (100) shows fundamental peaks.

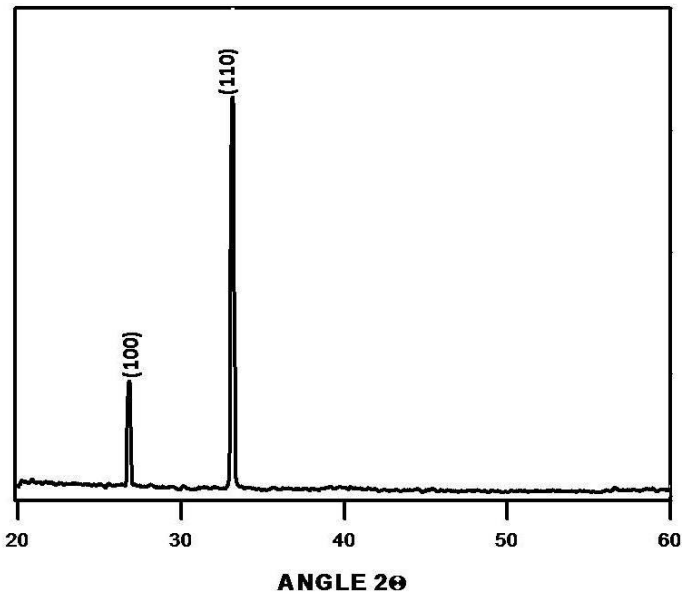

FIGURE 4.5 XRD of FePt nanoparticle made by SDS as surfactant.

The crystal structure of the FePt nanoparticles in a thin assembly was determined by the X-ray diffraction (XRD). The XRD of the as-synthesized FePt particles reveals a typical chemically disordered fcc structure,in which Fe atoms are substituted into Pt positions and vice versa. Annealing induces the Fe and Pt atoms to rearrange into the long range chemically ordered fct structure, which can be viewed as a natural superlattice of alternating Fe and Pt atomic planes. The change of the internal particle structure upon annealing depends on annealing temperature and duration, as well as the Fe/Pt ratio. The onset of this phase change occurs at about 600 °C.

4.2.2 MAGNETIC PROPERTIES OF THE NANOPARTICLE

Now there is **VSM** graph **Figure 4.6 (A)** of the as synthesized **FePt** Nanoparticle by using **SDS** as surfactant nanoparticle which shows that these particles have ferromagnetic characteristic at room temperature. And **Figure 4.6 (B)** which is magnified image of figure 4.6 (A) shows that it has coercivity and remanence which is nearly 129 Oe and 1.66 emu respectively.

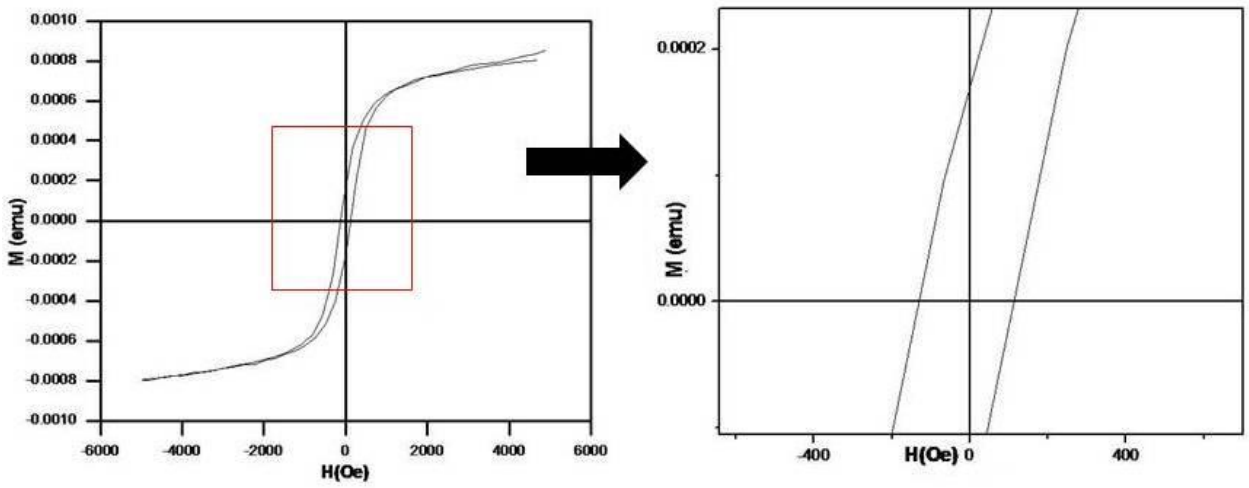

(A) **(B)**

Figure 4.6 Shows VSM result of FePt nanoparticle made by SDS as surfactanat nanoparticle **(A)** shows M-H graph of FePt by SDS **(B)** magnified image of figure 4.6 (A) to show coercivity and remanence.

4.3 EPR measurements OF FePt NANOPARTICLE:

Figure 4.7 shows the ELECTRON PARAMAGNETIC RESONANCE (EPR) spectra of FePt nanoparticles ,which shows that as synthesized nanoparticle are superparamagnetic at room temperature. Here g value is 2.00410, $\Delta Hpp = 154$ G, $H_{Res} = 3425.2$ G.

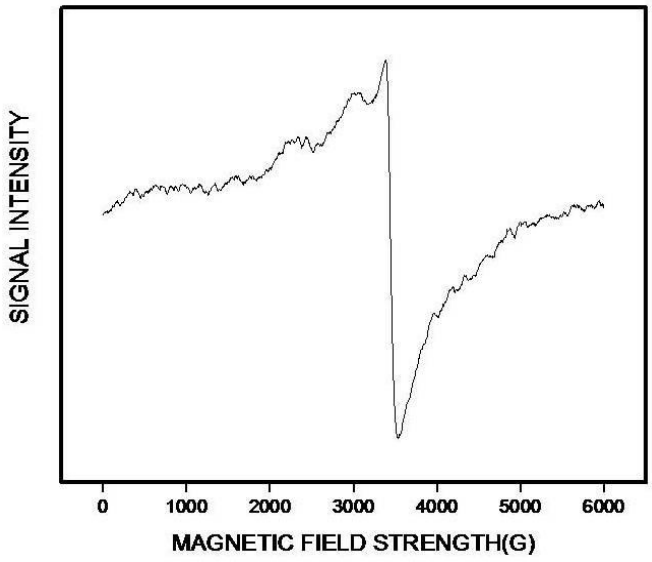

Figure 4.7 EPR Image of FePt nanoparticle made by super hydride reduction at high temperature showing superparamagetic behavior of nanoparticle.

4.4 POLYMER MEDIATED PEI/FePt NANOPARTICLE:

The oleic acid/oleylamine coated FePt nanoparticles can be readily dispersed into hexane or chloroform solvent, facilitating surface ligand exchange and controlled nanoparticle assembly. The ligand exchange experiments show that various functional polymers can replace oleic acid/oleylamine around these nanoparticles to give polymer nanoparticle composites. For example, mixing a chloroform solution of polyethylenimine (PEI) with a hexane dispersion of FePt led to the PEI-FePt nanocomposite that is not soluble in hexane. By exchanging the stabilizers bound to the particles with multifunctional polymers that attach to a substrate, the polymer and FePt nanoparticles can be alternately adsorbed onto the substrate, and an FePt assembly with controlled thickness can be made.

This polymeric moleculeassisted nanoparticle assembly is a well-known technique to produce polymer nanoparticle nanocomposites.[40-41] A densely packed self-assembled polymeric monolayer is usually obtained by spontaneous adsorption of surfactant molecules from organic solution onto a solid substrate via hydrogen bonding, ionic bonding, or covalent bonding. PEI has been found to be adsorbed on a HO-terminated substrate and is often used for gold or silica particle assembly on mica, silicon oxide and glass surfaces.[42,43]

The assembly of FePt nanoparticles into a macroscopic two-dimensional array on a PEI-functionalized substrate is depicted in **Figure 4.8**.[44] The assembly process includes **(1)** surface functionalization with a layer of PEI coating and **(2)** replacement of the particle stabilizers with a pendant functional -NH- group of the PEI. The pendant functional group –Nhextends out in the solution. By dipping the PEI-derivative substrate into the particle dispersion, ligand exchange at the PEI surface occurs and a monolayer FePt particle assembly is formed.

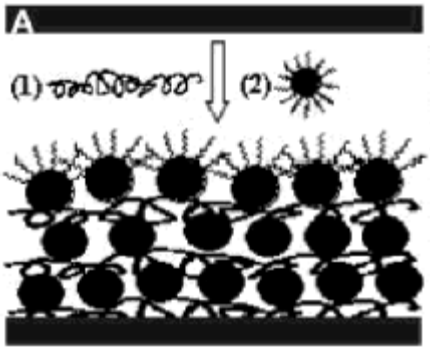

(A)

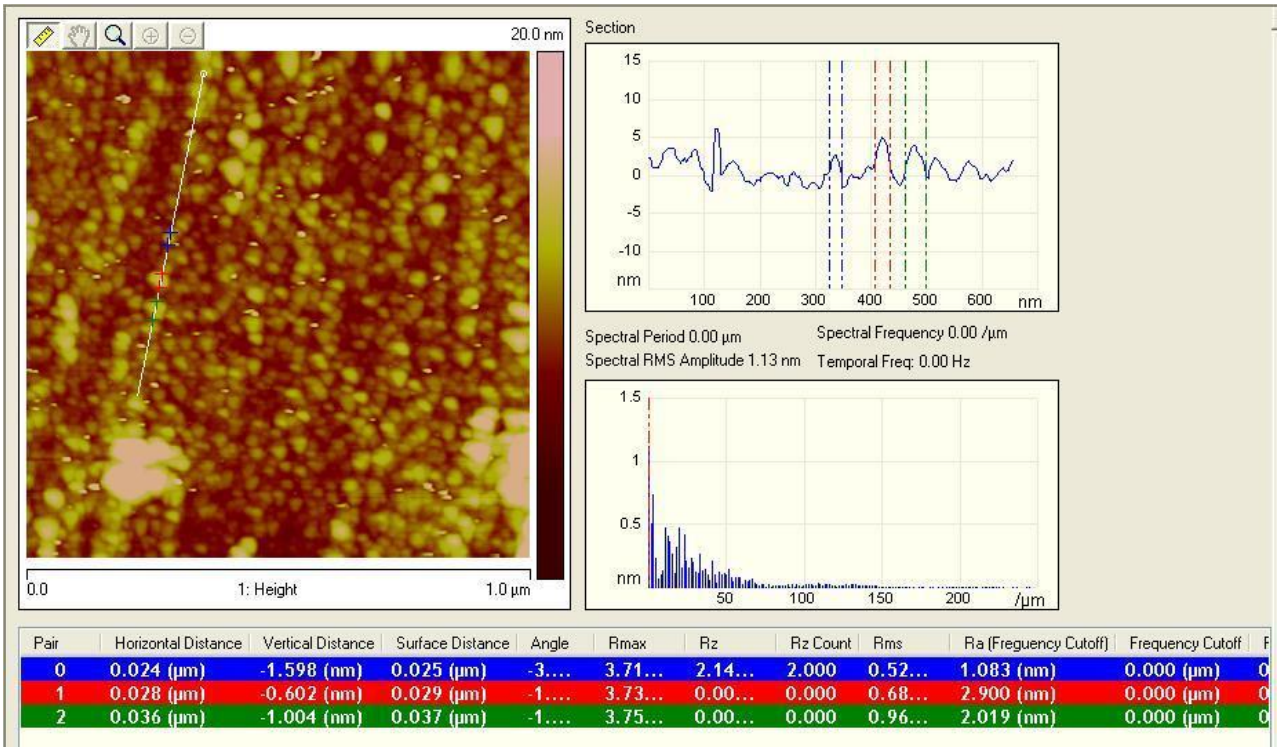

(B)

Figure 4.8 Schematic illustration of polymer-mediated self-assembly of FePt nanoparticles **(A)** by alternately adsorbing a layer of polymer (PEI) and a layer of nanoparticles on a solid surface.(1) Polymer,(2) FePt nanoparticle**. (B) AFM** results of assembly.

Figure (B) shows AFM image which shows the smoothness of the particle which is at 1.08nm.

4.5 ANNEALING OF FePt/PEI ASSEMBLY:

Annealing induces the Fe and Pt atoms to rearrange into the long range chemically ordered fct structure, which can be viewed as a natural superlattice of alternating Fe and Pt atomic

planes. The change of the internal particle structure upon annealing depends on annealing temperature and duration, as well as the Fe/Pt ratio. The onset of this phase change occurs at about 600 °C, which is consistent with the previous observation on FePt nanoparticles prepared from the decomposition/reduction process.

Figure 4.9 shows the typical superlattice peaks of (001) and (110) that are characteristic of the ordered FePt (L10) compound phase.

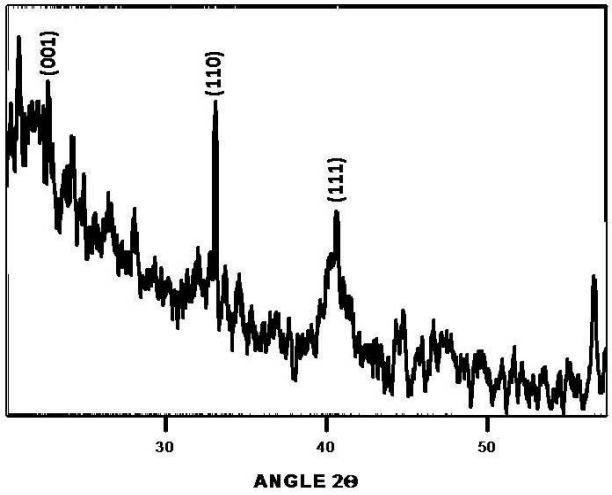

Figure 4.9 XRD of annealed FePt/PEI assembly for the one annealed for 30 min at 600 °C in N_2

CONCLUSION

In conclusion, FePt nanoparticles with particle size of 2 nm with narrow size disribution have been successfully synthesized by a polyol reduction process. The size control was achieved by adjusting synthesis parameters such as the surfactant to Pt precursor ratio, precursor ligands and reactor heating rate. Hysterisis loop and EPR spectroscope shows superparamagnetic behaviour of nanoparticle. The as-synthesized FePt nanoparticles have chemically disordered fcc structure that can be transformed into chemically ordered fct structure through thermal annealing. Moreover, a simplified and cost effective synthetic route has been found that provides a straightforward synthesis of FePt nanoparticles.

Synthesis through aqueous route is simple and safe due to it is low temperature method. The as-synthesized particles have uniformity in size with particle diameters of approximately 3 nm.Hysterisis loop shows ferromagnetic behavior of nanoparticle.

Structural and magnetic characterization show that FePt nanoparticles synthesized through this simplified method can provide the magnetically anisotropic L10 FePt phase with high coercivity in the form of thin film then the as synthesized FePt nanoparticle powder after thermal treatment.

Direct application of fully converted fct FePt nanoparticles in magnetic recording media and biomedical experiments is now possible. Based on a simple and economic processing feasible for industrial scale-up production, this technique can be also applied to production of other isolated materials structures where heat treatments, but not sintering, are required.

ADDITIONAL WORK AT NPL

SILICON NANOWIRES

INTRODUCTION:

Thermoelectric device interconverts thermal gradient and electricity for power generation or cooling [45-47]. Traditionally, Bi_2Te_3 semiconductor has been widely used as thermoelectric material due to its high thermoelectric performance, which has $ZT = a^2\sigma T/\kappa \approx 1$, where a, σ, κ and T represent Seebeck coefficient, electrical conductivity, thermal conductivity and absolute temperature, respectively [48-49]. However, thermoelectric devices based on Bi_2Te_3 are difficult to miniaturize. In addition, according to the late tendency of development and production of products using Bi_2Te_3 thermoelectric devices, supplies of Bi_2Te_3 are predicted to face shortage soon. On the contrary, silicon is the most abundant semiconductor material with the matured fabrication infrastructure. One drawback in the consideration of silicon as thermoelectric material is the low ZT value (≈ 0.01) due to its high κ value (≈ 150 $Wm^{-1}K^{-1}$) at room temperature [50-51]. Thus, silicon has been considered as the impropriate material for the thermoelectric applications. However, recent research revealed the possibility of silicon as thermoelectric material by incorporating nanotechnology. One-dimensional (nanostructured) silicon nanowire can dramatically reduce the phonon propagation through the nanowire while maintaining the electron/hole propagation property [52-54].

EXPERIMENTAL:

EE process begins with the cleaning of silicon substrates. 400 μm thick, polished silicon wafers having different doping types (n-type, p-type), resistivities (1–10 Ωcm) and crystallographic orientations (100, 111) were selected as the starting substrates. All chemicals were purchased from Sigma Aldrich and used without further purification. For cleaning, silicon substrates were consecutively sonicated in acetone (99.8%), isopropanol (99.8%) and deionized water baths for 10 min. As the final part of cleaning, piranha solution was prepared by mixing

sulfuric acid (H_2SO_4, 95–97%) and hydrogen peroxide (H_2O_2, 35%) in a 3:1 volume ratio and the samples were immersed in this solution for 30 min.

METHODOLOGY:

The samples were then dipped into dilute hydrofluoric acid (HF, 38–40%) solution for 2 min to remove the native oxide and allow the substrate surface to become hydrophobic. The EE solution was then prepared in a Teflon beaker containing 0.02 M $AgNO_3$ (99.5%) and 4.8 M HF (38–40%), in ratio of 1:1 and wafer then put in to this solution for 60 sec.

After the deposition of the metal particles, the sample wafer was immersed in an oxidizing HF etching solution (4.8M HF acid and 0.44M H_2O_2) in the ratio of 1:10 for 50 min, then wafer is rinsed with deionized water and dried at room temperature. The wafers were then cleaned in diluted HNO_3 so as to remove Ag particles.

RESULT AND DISCUSSION:

As the homogeneously dispersed silver ions come into contact with the substrate surface, these galvanic reactions take place simultaneously, and as a result, silicon is lost into the solution as SiF6, leaving pits on the wafer surface. These reactions selectively take place on the region where etching has already initiated and, as a consequence of this selective growth of holes throughout the surface, the remaining structure becomes vertically aligned arrays of Si NWs covered with silver (Ag) dendrites.

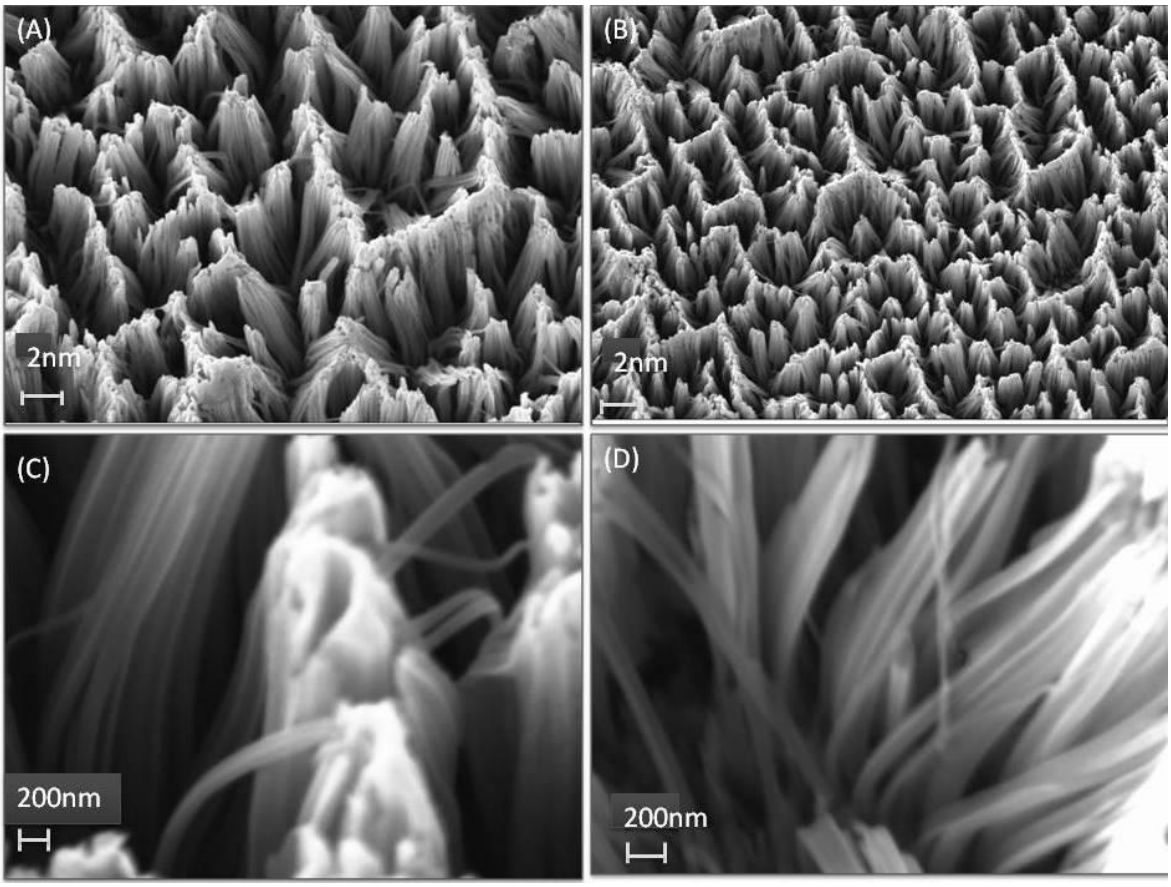

FIG 1 (A), (B),(C),(D) Shows **SEM** Image of Si nanowires with Different resolution.

FUTURE WORKS

Part 1

(1) Synthesized FePt nanoparticles by organic as well as aqueous route. Have done all the required characterization.

(2) Formed PEI/FePt anoparticle assembly and annealed it at high temperature.

(3) Magnetic measurement of the assembled film. To analyse the difference in the properties of assembled nanoparticles and powdered samples

(4) Since, for nanoparticles to store magnetic information at density over 100 Gbit/in2, they have to be arranged in a smooth thin assembly with a thickness of nearly 10nm[55]

Part II

(1) Silicon nanowires has been synthesized.

(2) The future work includes studying the thermoelectric properties and enhancing this property by graphene binding to SiNW's because CNT 's due to high aspect ratio and large surface area possess exciton dissociation and charge carrier transport properties. The core-shell nanostructure of SiNW-CNT improves the power conversion efficiency to be used in third generation solar cells and optoelctronic devices.

APPENDIX

(A) UNITS OF MAGNETIC

Quantity	Symbol	Gaussian & cgs emu	Conversion factor, C [b]	SI & rationalized mks [c]
Magnetic flux density, magnetic induction	B	gauss (G) [d]	10^{-4}	tesla (T), Wb/m^2
Magnetic flux	M	maxwell (Mx), Gθ cm^2	10^{-8}	weber (Wb), volt second (Vθs)
Magnetic potential difference, mangetomotive force	U, F	gilbert (Gb)	$10/4\pi$	ampere (A)
Magnetic field strength, magnetizing force	H	oersted (Oe), [e] Gb/cm	$10^3/4\pi$	A/m [f]
(Volume) magnetization [g]	M	emu/cm^3 [h]	10^3	A/m
(Volume) magnetization	$4\pi M$	G	$10^3/4\pi$	A/m
Magnetic polarization, intensity of magnetization	J, I	emu/cm^3	$4\pi\times10^{-7}$	T, Wb/m^2 [i]
(Mass) magnetization	σ, M	emu/g	1 $4\pi\times10^{-7}$	$A\theta m^2/kg$ Wbθm/kg
Magnetic moment	m	emu, erg/G	10^{-3}	$A.m^2/kg$, joule per tesla (J/T)
Magnetic dipole moment	j	emu, erg/G	$4\pi\times10^{-10}$	Wbθm [i]
(Volume) susceptibility	χ, κ	dimensionless, emu/cm^3	4π $(4\pi)^2\times10^{-7}$	dimensionless henry per meter (H/m), Wb/(Aθm)
(Mass) susceptibility	χ_ρ, κ_ρ	cm^3/g, emu/g	$4\pi\times10^{-3}$ $(4\pi)^2\times10^{-10}$	M^3/kg $H\theta m^2/kg$
(Molar) susceptibility	χ_{mol}, κ_{mol}	cm^3/mol, emu/mol	$4\pi\times10^{-6}$ $(4\pi)^2\times10^{-13}$	m^3/mol $H\theta m^2/mol$
Permeability	μ	dimensionless	$4\pi\times10^{-7}$	H/m, Wb/(Aθm)
Relative permeability [j]	μ_r	not defined		dimensionless
(Volume) evergy density, energy product [k]	W	erg/cm^3	10^{-1}	J/m^3
Demagnetization factor	D, N	dimensionless	$1/4\pi$	dimensionless

a. Gaussian units and cgs emu are the same for magnetic properties. The dfining relation is $B=H+4\pi$.
b. Multiply a number in Gaussian units by C to convert it to SI (e. g., 1 $G\times10^{-4}$ T/G=10^{-4} T).
c. SI (Système International d' Unités) has been adopted by the National Bureau of Standards. Where two conversion factors are given, the upper one is recognized under, or consistent with, SI and is based on the definition $B=\mu_o(H+M)$, where $\mu_o=4\pi\times10^{-7}$ H/m. The lower one is not recognized under SI and is based on the definition $B=\mu_oH+J$, where the symbol I is often used in place of J.
d. 1 gauss=10^5 gamma (γ).
e. Both oersted and gauss are expressed as $cm^{-1/2}\theta g^{1/2}\theta s^{-1}$ in terms of base units.
f. A/m was often expressed as "ampere-turn per meter" when used for magnetic filed strength.
g. Magnetic moment per unit volume.
h. The designation "emu" is not a unit.
i. Recognized under SI, even though based on the definition $B=\mu_oH+J$. See footnote c.
j. $\mu_r=\mu/\mu_o=1+\chi$, all in SI. μ_r is equal to Gaussian μ.
k. $B\theta H$ and $\mu_oM\theta H$ have SI units J/m^3; MθH and $B\theta H/4\pi$ have Gaussian units erg/cm^3.

(B) FePt PHASE DIAGRAM

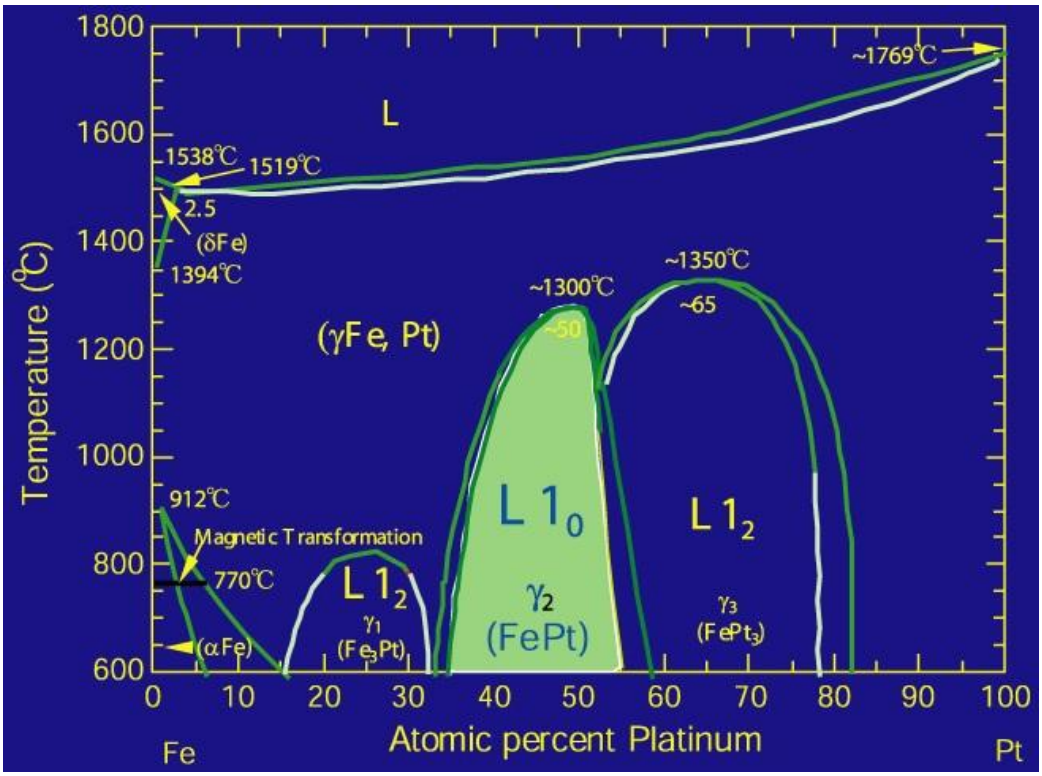

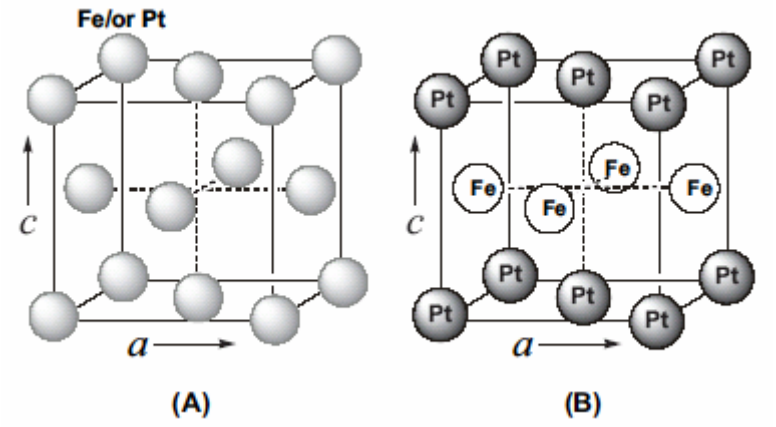

Figure B FePt phase diagram and schematic representation of structure transformation between **(A)** disordered fcc phase and **(B)** ordered fct phase.

(B) JCPDF FILE FOR FePt XRD

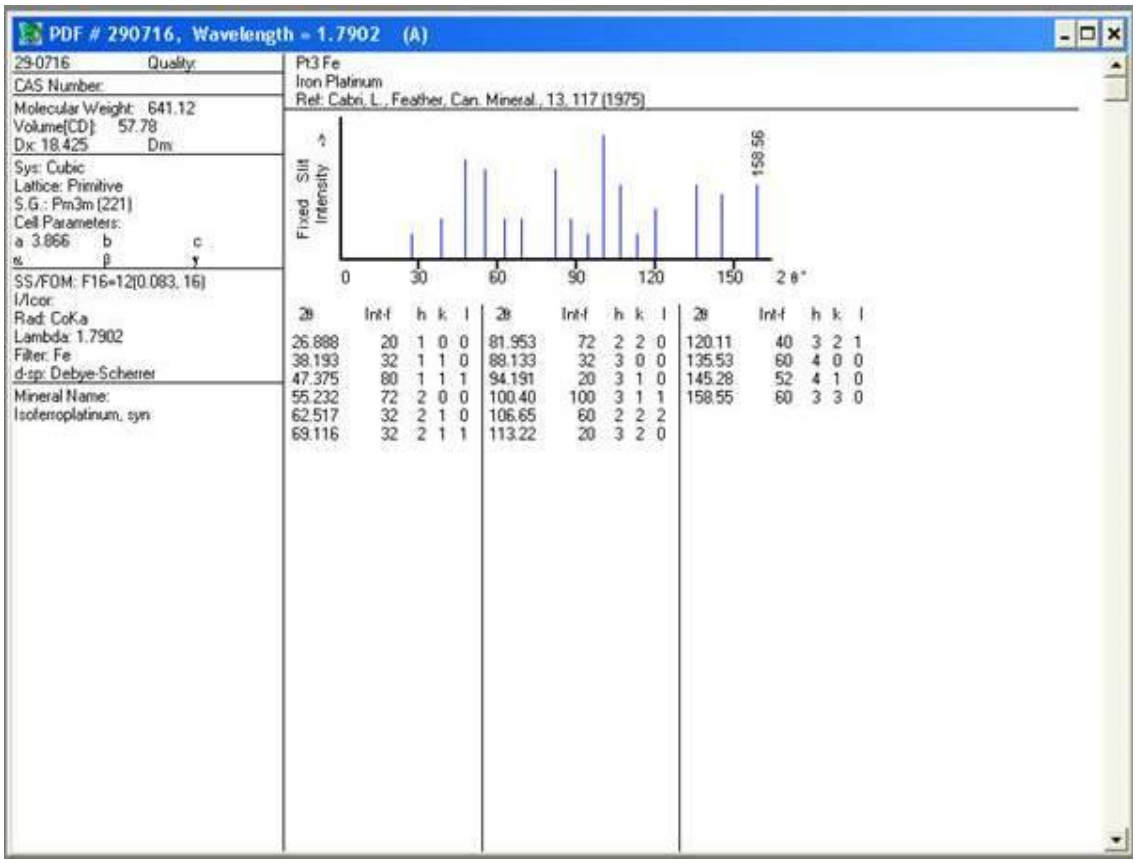

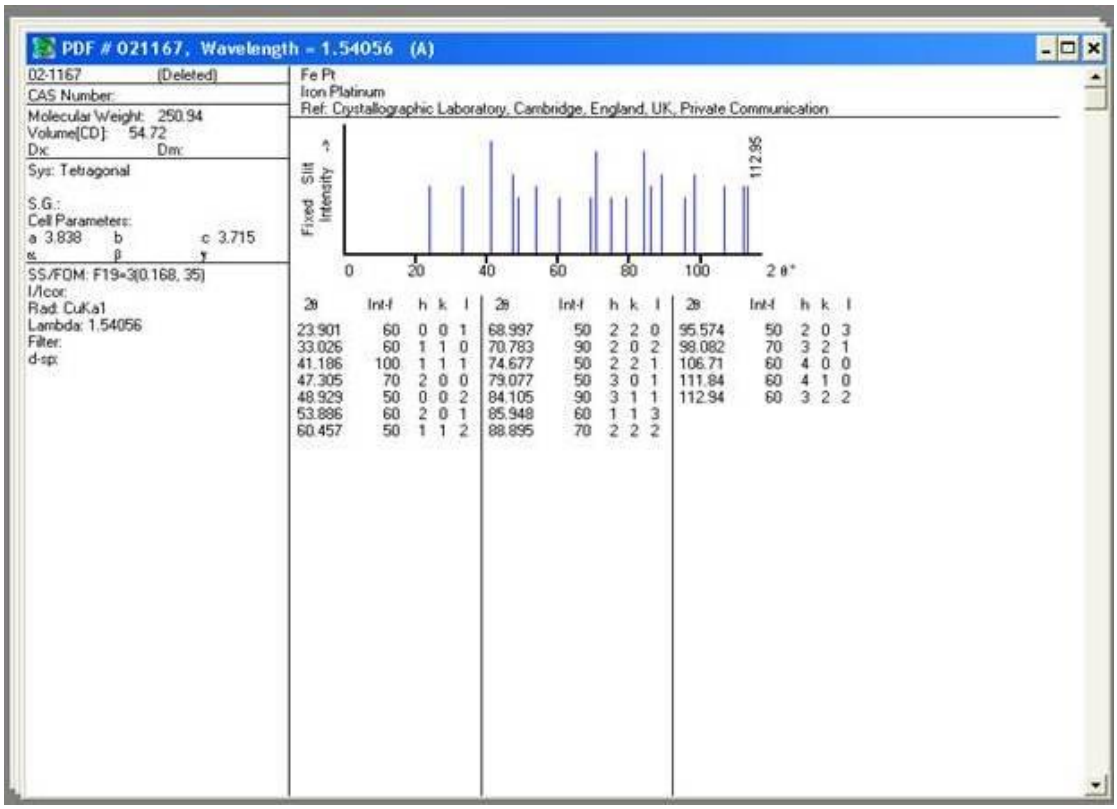

REFERENCES

[1] http://en.wikipedia.org/wiki/Magnet.

[2] http://www.arnoldmagnetics.com/mtc/index.htm.

[3] S. Chikasumi, "Physics of Magnetism", John Wiley and Sons 1964.

[4] B. D. Cullity, "Introduction to Magnetic Materials", Addison-Wesley Publishing 1972.

[5] Nicola A. Spaldn, " Magnetic Materials: Fundamentals and Device Applications", Cambridge University Press, 2003.

[6] R. C. O'handley, "Modern Magnetic Materials", A Wiley-interscience publication 2000.

[7] K. J. Klabunde, "Nanoscale Materials in Chemistry", John Wiley & Sons 2001.

[8] http://www.aacg.bham.ac.uk/magnetic_materials/

[9] Daren Li, Master thesis 2006.

[10] Eric E. Fullerton, J. S. Jiang, S. D. Bader, "Hard/Soft Magnetic Heterostructures: Model Exchange-Spring Magnets", Journal of Magnetism and Magnetic Materials, 200, 392 ,1999.

[11] http://www.azom.com/details.asp?ArticleID=637.

[12] E. F. Kneller, and R. Hawing "The Exchange-Spring Magnet: New Material Permanent Magnets", IEEE Transactions on Magnetics, 27, 3588 1991.

[13] C. Rong, H. Zhang, X. Du, J. Zhang, S. Zhang, and B. Shen, J. Appl. Phys., Vol. 96 3921, 2004.

[14] R. Skomski and J. D. D. Coey, Phys. Rev. B, 48, 15812,1993.

[15] C. Rong, H. Zhang, R. Chen, S. He, B. Shen, Journal of Magnetism and Magnetic Materials 302, 126–13,2006.

[16] B.D. Cullty, Elements of X-Ray Diffraction, Addison Wesley publishing co. Ind, London, 1967.

[17] J.W. Heal, J.T.Sparrow, P.M.Cross, in use of scanning electron microscopy, Pergaon Press, Oxford, 1972.

[18] W.R. Wenk, Electron Microscopy in mineralogy, Springer verlag, Berlin Heidelberg,Germany, 1976.

[19] P.B. Hirsch, A. Howie, P. B. Nicholson, D.W. Pashley, M.J. Whelen, Electron Microscopy of thin crystals , Butler worths, London, 1957.

[20] Odom, B.; Hanneke, D.; D'Urso, B.; and Gabrielse, G. ". *Physical Review Letters* **97** (3): 030801,"New Measurement of the Electron Magnetic Moment Using a One-Electron Quantum Cyclotron, 2006.

[21] The book by Wertz and Bolton has more information (pp. 46 and 442). Wertz, J. E., & Bolton, J. R. Electron spin resonance: Elementary theory and practical applications. New York: McGraw-Hill, 1972.

[22] "Dosimetry Systems". *Journal of the ICRU* **8** (5). 2008.

[23] Gualtieri, G.; Colacicchia, S, Sgattonic, R., Giannonic, M. *Applied Radiation and Isotopes* **55** (1): 71–79, "The Chernobyl Accident: EPR Dosimetry on Dental Enamel of Children". 2001.

[24] Chumak, V.; Sholom, S.; Pasalskaya, L. 1999.

[25] Baron, M., Chamayou, A., Marchioro, L., Raffi, J. *Adv. Powder Technol* **16** (3): 199–212, "Radicalar probes to measure the action of energy on granular materials". 2005.

[26] Schlesinger, H. I.; et al. *J. Am. Chem. Soc*, *84*, 1493, 1953.

[27] Yiping, L.; Hadjipanayis, G. C.; Sorensen, C. M.; Klabunde, K. J. *J. Magn. Mag. Mater*, *79*, 321, 1989.

[28] Glavee, G. N.; Klabunde, K. J.; Sorensen, C. M.; Hadjipanayis, G. C. *Langmuir*, *10*, 4726, 1994.

[29] Sun, Y.-P.; Rollins, H. W.; Guduru, R. *Chem. Mater*, *11*, 7, 1999.

[30] Bonnemann, H.; Brijoux, W.; Joussen, T. *Angew. Chem., Int. Ed. Engl*, *29*, 273,1999.

[31] Bonnemann, H.; Brinkmann, R.; Koppler, R.; Neiteler, P.; Richter, J. *Ad*V. *Mater*, *4*, 804, 1992.

[32]Sun, S.; Murray, C. B. *J. Appl. Phys.*, *85*, 4325,1999.

[33]Sun, S.; Murray, C. B.; Doyle, H. *Mater. Res. Soc. Symp. Proc*., *577*, 385, 1999.

[34] Sun, S.; Murray, C. B.; Weller, D.; Folks, L.; Moser, A. *Science* **2000**, *287*, 1989.

[35] Weller, D.; Sun, S.; Murray, C. B.; Folks, L.; Moser, M. *IEEE Trans. Magn*. *37*, 2185, 2001.

[36] Dai, Z. R.; Sun, S.; Wang, Z. L. *Nano Lett.*,*1*, 443,2001.

[37] Farrow, R. F. C.; et al. *J. Appl. Phys.*, *79*, 5967, 1996.

[38] Cebollada, A.; Farrow, R. F. C.; Toney, M. F. In *Magnetic Nanostructures*; Nalwa, H. S., Ed.; American Scientific Publishers: Stevenson Ranch, CA, p 93, 2002.

[39] Zeng, H.; Sun, S.; Vedantam, T. S.; Liu, J. P.; Dai, Z. R.; Wang, Z. L. *Appl. Phys. Lett.*, *80*, 2583, 2002.

[40] Fendler, J. H. *Chem. Mater*, *8*, 1616, 1996.

[41] Hicks, J. F.; Seok-Shon, Y.; Murray, R. W. *Langmuir*, *18*, 2288. 2002.

[42] Schmitt, J.; Ma¨chtle, P.; Eck, D.; Mo¨hwald, H.; Helm, C. A. *Langmuir*, *15*, 3256, 1999.

[43] Hua, F.; Cui, T.; Lvov, Y. *Langmuir*, *18*, 6712, 2002

[44] Sun, S.; et al. *J. Am. Chem. Soc.*, *124*, 2884, 2002

[45] D.M. Rowe, Thermoelectrics Handbook (CRC, Boca Raton, 2006)

[46] T.M. Tritt, M.A. Subramanian, MRS Bull. 31, 188 (2006)

[47] G.J. Snyder, E.S. Toberer, Nat. Mater. 7, 105 (2008)

[48] T.C. Harman, P.J. Tayor, M.P. Walsh, B.E. LaForge, Science 297, 2229 (2002)

[49] R. Venkatasubramanian, E. Siivola, T. Colpitts, R. O'Quinn, Nature 413, 597 (2001)

[50] B. Yang, J.L. Liu, K.L. Wang, G. Chen, Appl. Phys. Lett. 80, 1758 (2002)

[51] C.N. Liao, C. Chen, K.N. Tu, J. Appl. Phys. 86, 3204 (1999)

[52] A.I. Bouaki, Y. Bunimovich, J. Tahir-Kheli, J. Yu, W.A. Goddard III, J.R. Heath, Nature 451, 168 (2008)

[53] A.I. Hochbaum, R. Chen, R.D. Delgado, W. Liang, E.C. Garnett, M. Najarian, A. Majumdar, P. Yang, Nature 451, 163 (2008)

[54] D. Li, Y. Wu, R. Fan, P. Yang, A. Majumdar, Appl. Phys. Lett. 83, 3186 (2003)

[55] Wood, R. *IEEE Trans. Magn*. 36,36. **2000**.